High resolution correlation of the Homerian carbon isotope excursion (Silurian) across the interior of the Midland Platform (Avalonia), UK

Ray, David; Jarochowska, Emilia ; Röstel, Philipp ; Worton, Graham; Munnecke, Axel ; Wheeley, James; Boomer, Ian

DOI:
10.1017/S0016756819001146

Category: Original Article

High resolution correlation of the Homerian carbon isotope excursion (Silurian) across the interior of the Midland Platform (Avalonia), UK

David C. Ray[a]*, Emilia Jarochowska[b], Philipp Röstel[b], Graham Worton[c], Axel Munnecke[b] James R. Wheeley[a] and Ian Boomer[a]

*Corresponding author: daveray01@yahoo.com

[a]School of Geography, Earth and Environmental Sciences, University of Birmingham, Edgbaston, B15 2TT, United Kingdom

[b]GeoZentrum Nordbayern, Fachgruppe Paläoumwelt, Universität Erlangen-Nürnberg, Loewenichstr. 28, 91054 Erlangen, Germany

[c]Dudley Museum and Art Gallery. The Archives and Local History Centre, Tipton Road, Dudley, DY1 4SQ, United Kingdom

Short Title: **Homerian carbon isotope excursion**

Abstract

New $\delta^{13}C_{carb}$ and microfacies data from Hereford-Worcestershire and the West Midlands allow for a detailed examination of variations in the Homerian carbon isotope excursion (Silurian) and depositional environment within the Much Wenlock Limestone Formation of the Midland Platform (Avalonia), UK. These comparisons have been aided by a detailed sequence stratigraphic and bentonite correlation framework. Microfacies analysis has identified regional differences in relative sea-level change and indicates an overall shallowing of the carbonate platform interior from Hereford-Worcestershire to the West Midlands. Based upon the maximum $\delta^{13}C_{carb}$ values for the lower and upper peaks of the Homerian carbon isotope excursion (CIE) the shallower depositional setting of the West Midlands is associated with values that are 0.7‰ and 0.8‰ higher than in Hereford-Worcestershire. At the scale of parasequences the effect of depositional environment upon $\delta^{13}C_{carb}$ values can also be observed, with a conspicuous offset in the position of the trough in $\delta^{13}C_{carb}$ values between the peaks of the Homerian CIE. This offset can be accounted for by differences in relative sea-level change and carbonate production rates. While such differences complicate the use of CIEs as a means of high-resolution correlation and caution against correlations based purely upon the isotopic signature, it is clear that a careful analysis of the depositional environment can account for such differences and thereby improve the use of carbon isotopic curves as a means of correlation.

Key Words: carbon isotope stratigraphy, microfacies, Much Wenlock Limestone Formation, high-resolution correlation

1. Introduction

The stratigraphic variation of the $^{13}C/^{12}C$ values in marine carbonate ($\delta^{13}C_{carb}$) is increasingly used as a correlation tool (Saltzman & Thomas, 2012) with carbon isotopic excursions, such as the pronounced negative carbon isotope excursion (CIE) at the Ypresian GSSP (base Eocene) (Vandenberghe *et al*. 2012), used as the primary means of global correlation. Similarly, where key stratigraphic boundaries remain undefined (e.g. large parts of the Cambrian (Peng & Babcock, 2011)) or useful biostratigraphic markers are facies dependent (e.g. conodonts and graptolites within the Ordovician and Silurian (Bergström *et al*. 2012)) the identification and correlation of CIEs has significantly aided our ability to correlate. Indeed, our knowledge of the carbon isotopic record is such that standard $\delta^{13}C_{carb}$ curves are available for much of the Phanerozoic, including the Silurian (Cramer *et al*. 2011; Melchin *et al*. 2012). However, the generalised character of these standard curves masks significant local variations in the magnitude and morphology of many CIEs (e.g. Buggisch & Mann, 2004, figs. 12 and 13; Price *et al*. 2016, figs. 6 and 8). In particular, sedimentation upon carbonate platforms is typically dominated by biogenic benthic shallow-water carbonate producers, with the associated heterogeneity of carbonate platforms (e.g. lagoons, shoals, intershelf basins, barrier reefs, patch reefs) resulting in much local isotopic variability. These local isotopic variations are principally related to palaeobathymetry and its impact upon the types of carbonate producers, carbonate sedimentation and production rates and the exchange of waters between isotopically different reservoirs (e.g. open-ocean versus epicontinental seas), as well as secondary diagenetic processes (e.g. Holmden et al. 1998; Weissert *et al*. 2008; Da Silva & Boulvain, 2008; Swart, 2008; Saltzman & Thomas, 2012). For example, within the Silurian Baltic Basin absolute $\delta^{13}C_{carb}$ values of the Homerian Carbon Isotope Excursion are generally observed to decrease with increasing palaeobathymetry, with peak values above 4‰ within lagoonal settings decreasing to below 1‰ within the outer shelf (Jarochowska & Munnecke, 2015). While these changes are geographically rather gradual across the low-relief ramp topography of the Baltic Basin (on average −1‰ per 100 km within the East Baltic), the localised response of carbonate factories to episodes of sea-level change can result in rapid temporal and spatial changes in paleobathymetry and isotopic values. For example, a sea-level fall may result in the rapid progradation of isotopically heavier shallow marine carbonates into a deeper-water isotopically lighter setting. Similarly, a sea-level rise may result in all or parts of the carbonate platform back-stepping, giving-up, catching-up or keeping-up, each with their own influence on paleobathymetry and isotopic values. Thus, the local responses of a carbonate platform to sea-level change will result in local isotopic variations and hinder our ability to clearly establish the onset, termination and internal subdivisions of CIEs and therefore our ability to correlate CIEs.

Here we demonstrate the carbon isotope variability associated with a well-known Silurian CIE (Homerian Carbon Isotope Excursion; also termed the Mulde Carbon Isotope Excursion by some authors), as expressed on a relatively small Silurian carbonate platform (Midland Platform, Avalonia) and within an age synchronous platform interior carbonate succession (Much Wenlock Limestone Formation) (Fig. 1). Based upon a high-resolution sequence stratigraphic and bentonite framework it is apparent that local variations in relative sea-level influence the magnitude and morphology of the carbon isotopic record ($\delta^{13}C_{carb}$) within marine carbonate rocks.

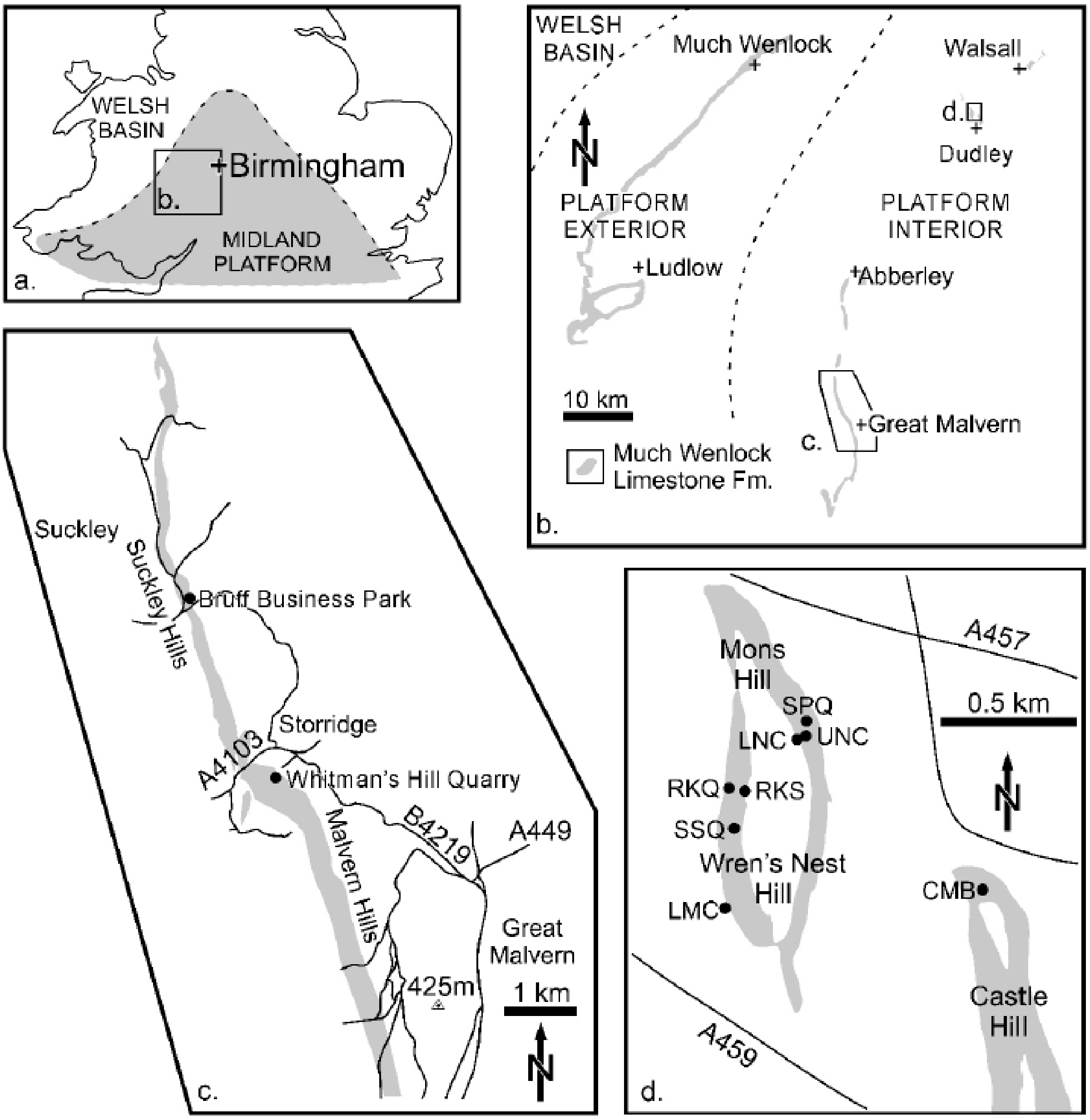

Figure 1. Locality maps for the Midland Platform. (a) Areas attributed to the Midland Platform and Welsh Basin showing the broad location of the study area. (b) Outcrop of the Much Wenlock Limestone Formation across the northern and central part of the Midland Platform with study areas located. (c) The Storridge and Suckley (Hereford-Worcestershire) areas showing the location of measured sections at Whitman's Hill Quarry (SO 7490 4830) and Bruff Business Park (SO 7365 5065); d. the Dudley (West Midlands) area showing the location of measured sections at Castle Hill, Wren's Nest Hill and Mons Hill: Castle Mill Basin (CMB) (SO 9454 9164), Reef Knoll Stairwell (RKS)

(SO 9363 9202), Lower NCC Cutting (LNC) (SO 9380 9222), Seven Sisters Quarry North (SSQ) (SO 9358 9188), Upper NCC Cutting (UNC) (SO 9382 9222), Reef Knoll Quarry (RKQ) (SO 9356 9200 and SO 9358 9210), Snake Pit Quarry (SPQ) (SO 9383 9228) and Lion's Mouth Cavern (LMC) (SO 9354 9161).

2. Geological setting

The upper Wenlock Series (Homerian Stage) Much Wenlock Limestone Formation (MWLF) reflects shallow-marine mixed carbonate and siliciclastic deposition upon the gently subsiding Midland Platform of eastern Avalonia (Bassett *et al*. 1992). During Homerian times the Midland Platform was within the tropics, situated some 13° degrees south of the equator (Torsvik *et al*. 1993); as reflected by an abundance of tropical patch-reefs and a diverse fossil biota (Ratcliffe & Thomas, 1999; Ray & Thomas, 2007). In general terms the MWLF thins and shows diachroneity between the platform interior and its western margin with the Welsh Basin. Within the platform interior the MWLF achieves a thickness of 37 m to 57 m and broadly corresponds to the latest *Cyrtograptus lundgreni* to *Colonograptus ludensis* graptolite biozones (Fry *et al*. 2017). In addition, the MWLF has been subdivided into three members (Lower Quarried Limestone, Nodular Beds and Upper Quarried Limestone members) according to the relative abundances of limestone and silty-mudstone, with such variations broadly reflecting episodes of relative sea-level change. Lastly, the MWLF is under- and over-lain by thick successions of occasionally graptolitic silty-mudstone, the Coalbrookdale and Lower Elton formations respectively. The transitional facies between these silty-mudstones and the MWLF have been informally and locally referred to as the Basement Beds and Passage Beds (Butler, 1939), and their local inclusion in the MWLF has resulted in minor diachroneity across the platform interior.

As a means of removing this diachroneity and synchronising litho- and chrono-stratigraphy, we consider the locally identifiable Basement Beds as belonging to the uppermost Coalbrookdale Formation and the regionally identifiable Passage Beds as belonging to the uppermost MWLF.

Previous carbon isotope studies of the Midland Platform have documented the dual peaked Homerian CIE, with the most extensive records derived from the Silurian inliers of the Dudley, West Midlands (Corfield *et al*. 1992; Marshall *et al*. 2012). In addition, parts of the Homerian CIE have been documented elsewhere upon the Midland Platform, with records from the type Wenlock and Ludlow areas (Much Wenlock and Ludlow) being particularly important for age calibration (Blain *et al*. 2016; Fry *et al*. 2017).

2a. Stratigraphic precision within the study area

The ability to accurately resolve the stratigraphic record is critical to understanding past global change and the variability of the carbon isotopic record. Unfortunately, for the majority of Wenlock sections that document the Homerian CIE the stratigraphic resolution is below that required to test such variability, with the result that the peaks and troughs in the carbon isotopic record are considered near-isochronous and form the basis of correlation. However, high-resolution stratigraphic techniques such as the correlation of changes in sea-level caused by Milankovitch forcing of ice sheet dynamics and the correlation of volcanic ash layers can approach isochronous correlation, and can therefore be used to examine differences between local carbon isotopic curves.

The sections described herein are from the Dudley (West Midlands), Storridge and Suckley (Hereford-Worcestershire) areas and are considered characteristic of the platform interior (Fig. 1b), in that they reflect the earliest onset of the deposition of the MWLF, which begins with an interval of microbial carbonates (Lower Quarried Limestone Member) indicative of restricted circulation within a platform interior setting (Ratcliffe, 1988). Based upon comparison with the Geologic Time Scale 2012 (Melchin *et al*. 2012) and the alternative absolute age determinations of Cramer *et al*. (2012), the MWLF and the Homerian CIE likely equate to an interval of 0.6 to 1.9 million years, with a high-resolution radioisotopic date from near the top of the MWLF at Dudley providing an in situ upper absolute age limit of 427.86 ± 0.32 Ma (Cramer *et al*. 2012). Correlation between these sections (approximately 48 km between the most distal sections) has been achieved by means of high-resolution sequence stratigraphy and the geochemical correlation of a prominent volcanic ash horizon (bentonite) within middle of the formation.

The details of correlation across the study area are given in Ray et al. (2013), but are summarised here. In terms of sequence stratigraphy, the MWLF is represented by two regressive episodes separated by a marked transgression. These broad sea-level changes are well documented from a number of palaeocontinents (e.g. Avalonia, Baltica, Gondwana and Laurentia) and are considered to be eustatic in nature (e.g. Johnson 2006). The expression of these eustatic variations across the study area and the wider Midland Platform (e.g. Ray *et al*. 2010; Ray *et al*. 2013; Fry et al. 2017) allows the MWLF to be subdivided into sequence stratigraphic systems tracts (see Simmons, 2012) according to the rate and direction of sea-level change. Furthermore, each systems tract (i.e. transgressive, highstand and falling stage systems tracts) has been further subdivided into multiple upward shallowing cycles (parasequences), which can be distinguished from each other and correlated according to differences in thickness and the magnitude of relative sea-level change. Thus, sea-level trends may be observed through successive parasequences, and these stacking patterns reflect broader lithological trends that are expressed as systems tracts. Such correlations allow for the subdivision of the MWLF into twelve parasequences (PS1 to PS12), and based upon a 0.6 to 1.9 million years duration for the MWLF, suggest a mean parasequence duration in the order of 50 to 150 ka. Accordingly, it seems likely that the parasequences, being part of a broader eustatic trend, may be reflective of short eccentricity Milankovitch cycles of ~100 ka duration and therefore suitable for high-resolution correlation.

The sequence stratigraphic subdivision and correlation of the MWLF has been additionally confirmed by the geochemical fingerprinting and correlation of volcanic ash layers (bentonites; also termed K-bentonites or metabentonites by some authors). The correlation of bentonites within the MWLF is of particular significance in that the deposition of the bulk of volcanic ejecta can be considered instantaneous on geological timescales (see Huff 2016). Across the study area the presence of volcanic apatite crystals within the bentonites and the rare earth element (REE) geochemical signature of the apatite crystals has been used as a means of distinguishing between individual bentonites (Ray *et al*. 2013). In particular, apatite REE data from most bentonites within the MWLF probably originated from a granodiorite magmatic source, with the exception of a bentonite horizon within the middle of the formation that has a distinctively mafic composition; more akin to that of a gabbro or syenite. This distinctively mafic bentonite has been geochemically identified in sections at Dudley (Wren’s Nest Hill) and Storridge (Whitman’s Hill) and occurs in the flooding interval at the base of parasequence 8 (PS8), thereby confirming the near isochronous deposition of PS8, the highstand systems tract and the Nodular Beds Member. In addition, this bentonite is notably thicker than the majority of other bentonites (120-

200 mm) thereby allowing for easy identification in other sections across the area, including in the Bruff Business Park section (Ray *et al*. 2013).

Within the wider Wenlock of the Midland Platform bentonite geochemistry has also been used to confirm the synchronicity of sequence stratigraphic correlations. For example, a bentonite has been correlated within the MWLF from Dudley (West Midlands) to Wenlock Edge (Shropshire) and confirms the correlation of PS10 over a distance of approximately 40 km (Ray et al. 2011). Similarly, within the lower Wenlock a bentonite has been used to confirm the correlation of a parasequence (cycle 5) within the uppermost Buildwas and Woolhope Limestone formations, over a distance of 62 km (Hughes & Ray, 2016). Based upon these combined bentonite-sequence stratigraphic studies it is apparent that the parasequences of the Midland Platform represent discrete and approximately age synchronous depositional episodes that likely result from Milankovitch cycles (i.e. short eccentricity), and as such ideal for the comparison of carbon isotopic values across the study area.

3. Sampling and analytical methods

The succession of Hereford-Worcestershire has not previously been subject to detailed carbon isotopic analysis and has consequently formed the focus of our sampling efforts (Fig. 1c). The Whitman's Hill Quarry contains the uppermost Coalbrookdale Formation (15.8 m) and the lower two-thirds of the MWLF (24.4 m) and has been sampled in its entirety. Approximately 2.5 km north-northwest of Whitman's Hill is the Bruff Business Park section which contains the whole of the MWLF, as well as parts of the under- and over-lying formations. Owing to faulting near the base of the MWLF (Fig. 2) our sampling has focused upon the interval above this fault zone and immediately above a distinctively thick (120 mm) and a regionally traceable marker bentonite (WH9 of Ray *et al*. 2013). Accordingly, at Bruff Business Park the upper half of the MWLF (21.9 m) and the basal Lower Elton Formation (8.2 m) has been sampled. In combining samples from both Whitman's Hill Quarry and Bruff Business Park a local composite carbon isotope curve has been made and based upon the correlation of the marker bentonite and parasequences, there is an approximate sampling overlap of 6 m between sections. In terms of sedimentology, the results of hand-specimen analysis and a limited number of thin sections have previously been reported for the Hereford-Worcestershire succession (Penn, 1971; Ray *et al*. 2013; Päßler *et al*. 2014), alongside more regional studies (Phipps & Reeve, 1967). However, as a means of further improving our understanding of the succession, a number of thin sections were created to confirm and improve upon the existing sedimentological descriptions and to investigate intervals that show considerable regional variability and may consequently impact upon the local carbon isotopic signature.

Given the existing and detailed sedimentological (Butler, 1939; Oliver, 1981; Ratcliffe, 1988; Ratcliffe & Thomas, 1999; Ray & Thomas, 2007; Ray *et al*. 2010) and carbon isotopic records (Corfield *et al*. 1992; Marshall *et al*. 2012) from the Dudley area (West Midlands) a duplication of such works would superficially be of limited merit. However, a comparison of the carbon isotopic record of Corfield *et al*. (1992) and Marshall *et al*. (2012) reveals some differences in the shape of the resultant curves. Furthermore, while only the curve of Marshall *et al*. (2012) has been linked to the available sequence stratigraphic record, it has been shown by Blain *et al*. (2016, p 729) that there may be a degree of uncertainty as to the exact position of the carbon isotopic data and the parasequences identified by Ray *et al*. (2010). Finally, both curves are based upon sections which contain minor faulting, particularly at the lower and upper boundaries of the MWLF, and are also reliant on accurate correlation between sections. In the case of the Corfield *et al*. (1992) it is apparent that the use of the trench and quarry face on the eastern side of Wren's Nest Hill (SO 9382 9220) would have likely resulted in approximately 5 m of the uppermost Nodular Beds Member being unaccounted for in their curve (Ray *et al*. 2010, p 139).

While the previously published carbon isotope curves demonstrate the broad nature of the Homerian CIE, it is unclear how accurately they relate to the parasequences established within the Dudley area, and therefore with the data collected from Hereford-Worcestershire. Thus, in order to confirm the isotopic trends within each parasequence we have resampled the succession. In particular, we have undertaken high-resolution sampling (typically 0.20 m or less) across the formation boundaries (Coalbrookdale, Much Wenlock Limestone and Lower Elton formations) and somewhat lower-resolution sampling (typically every 0.50 m) for the remainder of the succession. Such a sampling strategy is intended to improve upon the stratigraphic resolution of the onset and termination of the Homerian CIE (across the formation boundaries), as well as to determine the broad isotopic trend within the remainder of the succession.

Alongside isotopic sampling within the Dudley area a limited number of thin sections were created to improve upon previous descriptions (e.g. Oliver, 1981; Ratcliffe, 1988; Ratcliffe & Thomas, 1999) and link more precisely to the sequence stratigraphic units described by Ray *et al*. (2013). In particular, we have focused upon the Basement and Passage beds as these represent intervals of significant lithological and environmental change.

After collecting limestone samples from the Hereford-Worcestershire and West Midlands areas, stable carbon and oxygen stable isotope measurements were carried out in the stable isotope laboratory of the GeoZentrum Nordbayern, Erlangen, Germany. Unweathered samples of vein-free bulk rock were powdered using a hand drill. This method of analysing bulk rock for stable isotopes, which inevitably does contain some skeletal material, has been shown to provide reliable results in other Silurian studies (e.g. Cramer *et al*. 2006; Kaljo & Martma, 2006; Hughes & Ray, 2016). The carbonate powders were reacted with 100% phosphoric acid at 70°C using a Gasbench II connected to a Thermo Finnigan Five Plus mass spectrometer. All values are reported in per mille relative to V-PDB by assigning $\delta^{13}C$ and $\delta^{18}O$ values of +1.95‰ and −2.20‰ to international standard NBS19 and −46.6‰ and 26.7‰ to international standard LSVEC, respectively. Reproducibility and accuracy were monitored by replicate analysis of laboratory standards calibrated to NBS19 and LSVEC and were better than ±0.06‰ (1σ) and ±0.04‰ (1σ), respectively. In total, 459 of the analysed samples provided geochemical results, typically at sample spacing of 0.1 to 0.5 m (Supplementary Material).

3.a. Whitman's Hill and Bruff Business Park carbon isotope stratigraphy

Carbon isotope values in the upper part of the Coalbrookdale Formation are rather variable and range between -1.3‰ and 1.8‰ $\delta^{13}C_{carb}$ (Fig. 2). Broadly there is a positive trend within the formation, but it is only within the uppermost 1.0 m that values start to exceed 1.0‰. Within the basal 0.9 m of the Lower Quarried Limestone Member (MWLF) (15.64-16.54 m) values increase from 0.9‰ to 4.6‰ and correspond to the onset of the Homerian CIE. This marked positive shift in values takes place within the basal parasequence (PS1) of the MWLF and a peak value of 4.8‰ is achieved in the overlying parasequence (PS2). From this peak (lower peak of the Homerian CIE), values progressively fall throughout the remainder of the Lower Quarried Limestone Member (PS2 to PS5) and into the Nodular Beds Member, as exposed at Whitman's

Hill (PS6 to basal PS10), with values falling to around 1.7‰ by the top of the section. Particularly notable features of this fall in values are its uniform nature and its occasional punctuation by more negative values, the most notable of which (occurs across multiple samples) is high within PS7.

At Bruff Business Park (Fig. 2) the overlapping part of the succession (PS8 to basal PS10) appears to show the continuation of the decline in values observed at Whitman's Hill. Based upon a consideration of both sections this trend ends around the PS9-PS10 boundary, above which values rise from 1.7‰ to 3.0‰ (Bruff Business Park 9.60-15.10 m) towards the top of PS10 and within the lower part of the Upper Quarried limestone Member. This peak corresponds to the upper peak of the Homerian CIE, above which values progressively fall throughout the remainder of the MWLF and into the basal Lower Elton Formation. Broadly the apparent rate of fall is greatest within the Passage Beds of the Upper Quarried Limestone Member (PS12) indicating that the Homerian CIE ends at the top of MWLF. Within the Lower Elton Formation values are still elevated when compared with the pre-excursion Coalbrookdale Formation and range from 1.0‰ to 1.9‰.

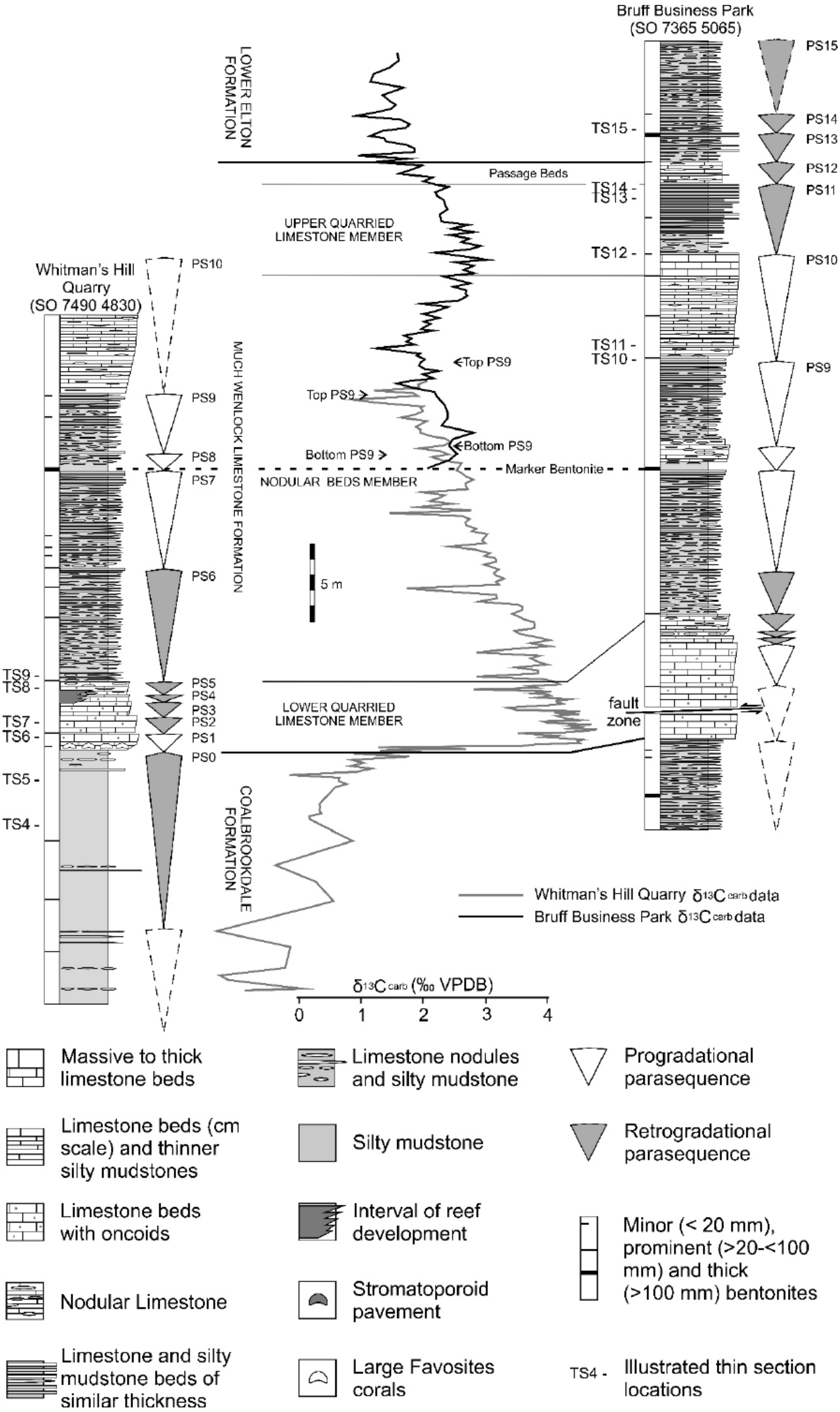

Bruff Business Park
(SO 7365 5065)
Whitman's Hill
Quarry
(SO 7490 4830)
LOWER ELTON FORMATION
Passage Beds
UPPER QUARRIED LIMESTONE MEMBER
MUCH WENLOCK LIMESTONE FORMATION
NODULAR BEDS MEMBER
LOWER QUARRIED LIMESTONE MEMBER
COALBROOKDALE FORMATION
Top PS9
Bottom PS9
Marker Bentonite
fault zone
5 m
PS0
PS1
PS2
PS3
PS4
PS5
PS6
PS7
PS8
PS9
PS10
PS11
PS12
PS13
PS14
PS15
TS4 -
TS5 -
TS6 -
TS7 -
TS8 -
TS9 -
TS10 -
TS11 -
TS12 -
TS13 -
TS14 -
TS15 -
Whitman's Hill Quarry δ13Ccarb data
Bruff Business Park δ13Ccarb data
δ13Ccarb (‰ VPDB)
0
1
2
3
4
Massive to thick limestone beds
Limestone beds (cm scale) and thinner silty mudstones
Limestone beds with oncoids
Nodular Limestone
Limestone and silty mudstone beds of similar thickness
Limestone nodules and silty mudstone
Silty mudstone
Interval of reef development
Stromatoporoid pavement
Large Favosites corals
Progradational parasequence
Retrogradational parasequence
Minor (< 20 mm), prominent (>20-<100 mm) and thick (>100 mm) bentonites
TS4 - Illustrated thin section locations

Figure 2. Stratigraphic overview of Whitman’s Hill Quarry and Bruff Business Park modified from Ray *et al*. (2013), showing the carbon isotopic values, the position of parasequences (PS), bentonite correlations (Marker Bentonite), lithostratigraphic units and transitional intervals (Passage Beds).

3.b. The Dudley area carbon isotope stratigraphy

The succession within the Dudley area (Castle Hill, Wren’s Nest Hill and Mons Hill) has been uplifted, folded and faulted during the Caledonian and the Variscan orogenies and outcrops in a series of discontinuous quarries. Consequently no one outcrop offers access to the entirety of the succession. Here we document both the carbon isotopic trends and the correlations necessary to stitch together this composite carbon isotope curve (Figs. 1d and 3).

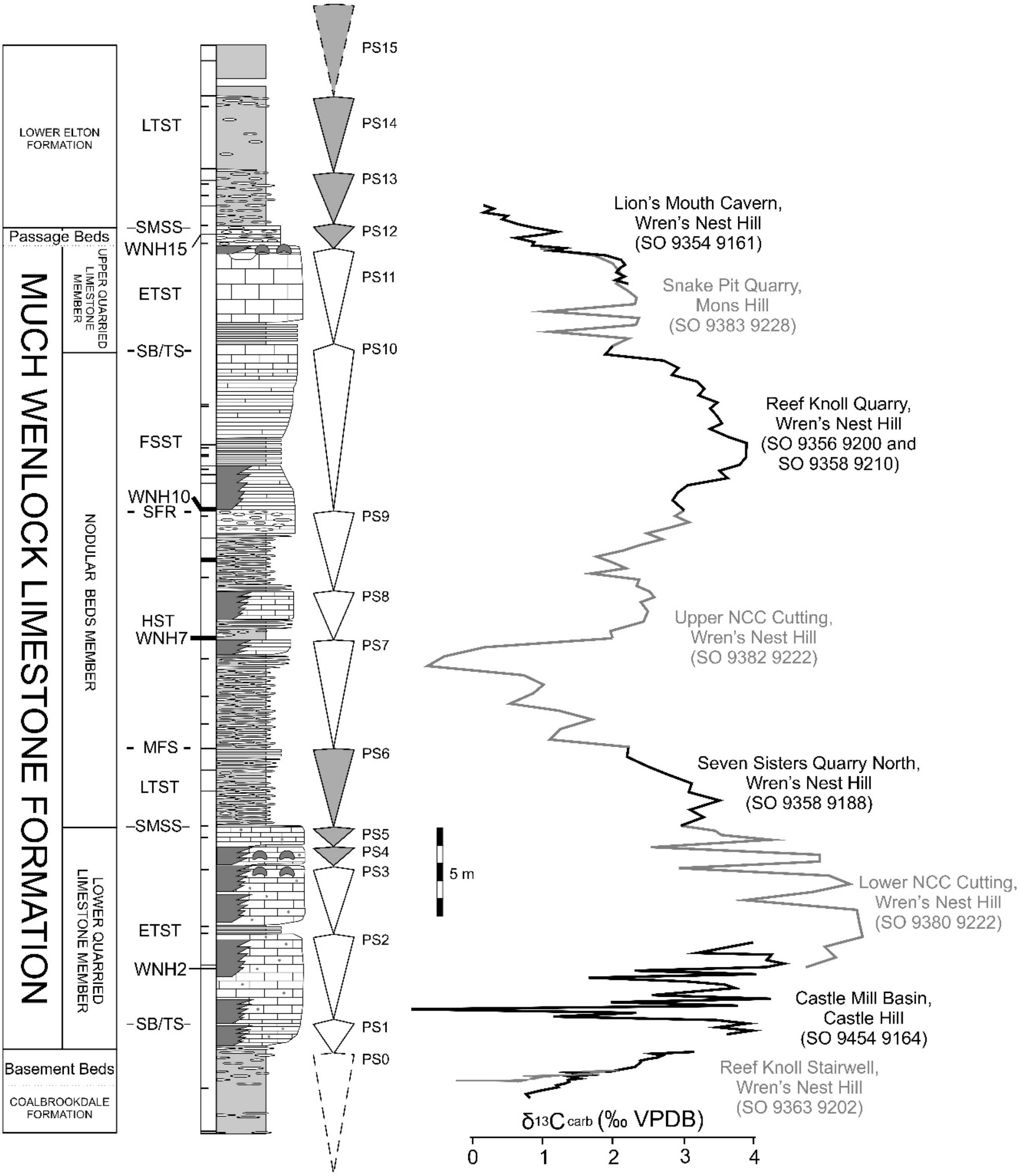

Figure 3. Stratigraphic overview of the Dudley area modified from Ray *et al*. (2013), showing the position of the measured sections, carbon isotopic values, the position of parasequences (PS), marker bentonite beds (WNH), lithostratigraphic units and transitional intervals (Basement and Passage beds) (see Figure 2 for the key). Within the study area are the following systems tracts and their bounding surfaces: SB/TS - sequence boundary and combined transgressive surface; ETST - early transgressive

systems tract; SMSS - surface of maximum sediment starvation; LTST - late transgressive systems tract; MFS - maximum flooding surface; HST - highstand systems tract; SFR - surface of forced regression; FSST - falling stage systems tract.

The stratigraphically lowest part of the succession has been investigated at the Castle Mill Basin (Castle Hill) and the Reef Knoll Stairwell (Wren's Nest Hill). Here the sections contain the transitional interval between the Coalbrookdale Formation and Lower Quarried Limestone Member (MWLF). In addition, as neither section was sampled by Corfield *et al*. (1992) or Marshall *et al*. (2012), they provide additional documentation of the onset of the Homerian CIE within the Dudley area.

The Castle Mill Basin succession is the most stratigraphically extensive of the sections (Fig. 4a, b) and one the most complete in the area (location CH12 of Butler, 1939). It begins within the uppermost Coalbrookdale Formation (2.60 m). The Coalbrookdale Formation isotopic values initially range from 0.8‰ to 1.7‰ $\delta^{13}C_{carb}$, before rising markedly from 1.4‰ to 3.1‰ within the Basement Beds. Unfortunately, a 1.00 m interval of no-exposure within the section corresponds to the boundary between the Coalbrookdale Formation and Lower Quarried Limestone Member, but values continue to rise into the lowest MWLF to an initial peak of 3.9‰ (3.80 m), above which the rate of rise is reduced. Such an arrangement indicates that the onset of the Homerian CIE broadly corresponds to the Coalbrookdale-Much Wenlock Limestone formation boundary, but begins in the uppermost Coalbrookdale Formation (Basement Beds). Stratigraphically above values briefly remain between 3.5‰ and 3.9‰, before dropping to -0.8‰ (5.00 m). This pronounced negative excursion occurs over a 0.8 m interval, above which values rebound and continue to rise to a maximum value of 4.2‰, all be it with significantly more variability (between 1.7‰ and 4.2‰); these isotopic variations are likely reflective of lithological variability in association with bioherms.

The Reef Knoll Stairwell sections contains only 0.68 m of the succession that approximates to the boundary between the Coalbrookdale Formation and the MWLF (Fig. 3). As with the Castle Mill Basin section, values show a marked increase in isotopic values with the stratigraphically lowest and highest values typical of this trend (0.7‰ to 2.1‰). Based upon a comparison with the absolute isotopic values taken from the Castle Mill Basin section, this small outcrop likely corresponds to a prominent grainstone lens within the Basement Beds, rather than the base of the Lower Quarried Limestone Member.

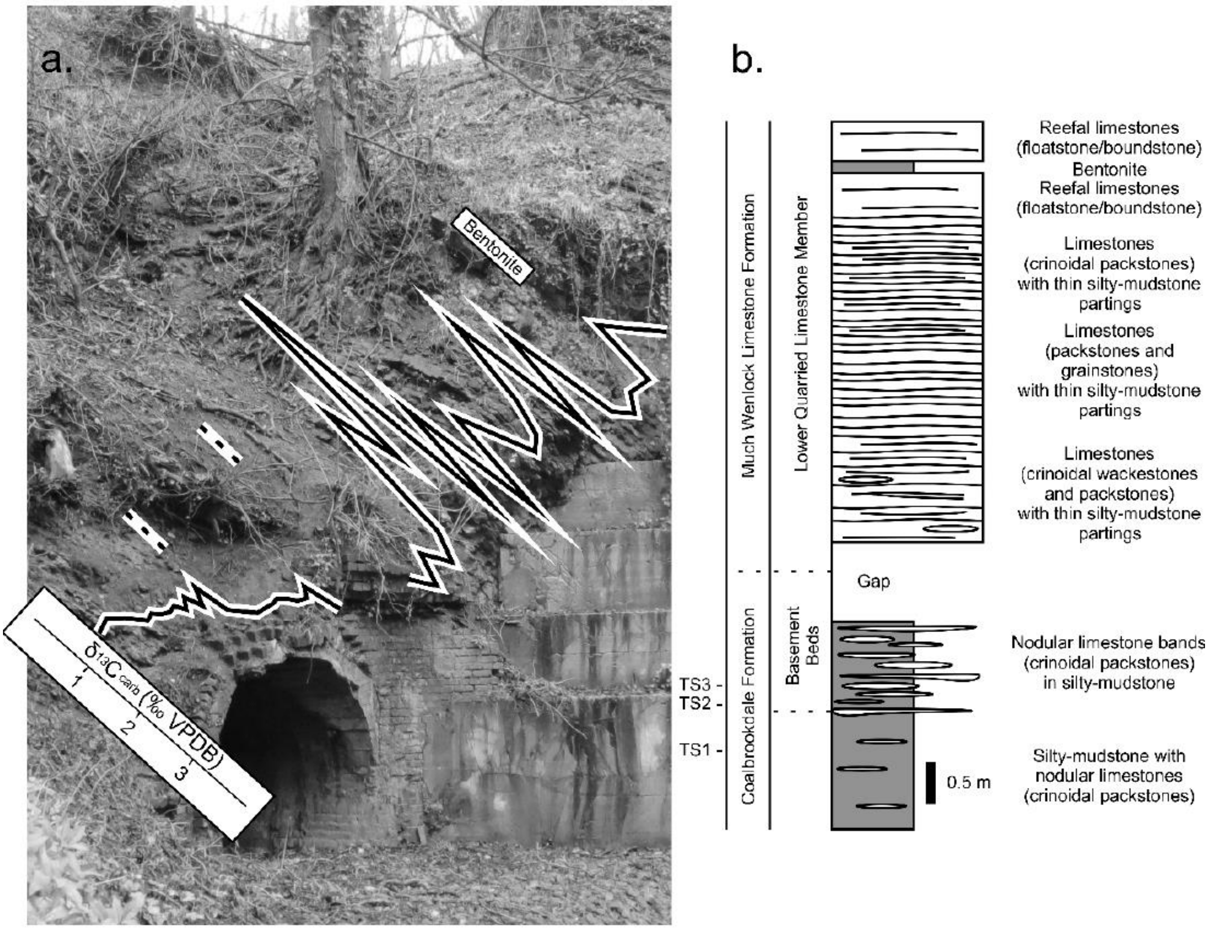

Figure 4. The carbon isotopic record across the Coalbrookdale-Much Wenlock

Limestone Formation boundary at Dudley. (a) The Castle Mill Basin section (Wren's Nest Tunnel Portal) and the carbon isotopic record. (b) Stratigraphic overview of Castle Mill Basin section.

Lower NCC Cutting at Wren's Nest Hill occurs at the northern end of a trench, cut to extract the Lower Quarried Limestone Member. This section contains minor faulting at the base of the Lower Quarried Limestone Member and in the immediately overlying Nodular Beds Member. Correlation with the Castle Mill Basin section has been achieved by the correlation of a bentonite (WNH2; Ray et al. 2011) between the sections. This bentonite and an immediately overlying bentonite are key markers within the Lower Quarried Limestone Member of the Dudley area and occur within PS2. In addition, measurements from the base of the Lower Quarried Limestone Member to the bentonite are consistent between the sections. This part of the isotopic curve begins immediately below the marker bentonite (WHN2) and shows a continued rise in $\delta^{13}C_{carb}$ values to 5.5‰ by the top of PS2. Above values initially plateau within PS3 before progressively declining (minimum value of 2.5‰) through to the top of PS5, the end of the measured section and the top of the Lower Quarried Limestone Member.

The boundary between the Lower Quarried Limestone and Nodular Beds member is commonly faulted and appears particularly unpromising in the Lower NCC Cutting. Of the sections available, a pillar in limestone workings near the Seven Sisters Caverns (Seven Sisters Quarry North) offers the most complete and accessible example of PS6 and the base of the Nodular Beds Member; despite some minor quarrying-related slumping at its base. Within PS6 the decline in $\delta^{13}C_{carb}$ values continue to a low of 2.2‰ by the top of the parasequence.

Parasequences 7 to 9 can be accessed in their entirety within the Upper NCC Cutting (a continuation of the Lower NCC Cutting above the faulted interval). Here values continue to decline to a clear trough within the upperpart of PS7 (minimum value of -0.6‰ at 4.00 m). Above values rapidly rise through the remainder of PS7 and peak in PS8 at 2.6‰. Values then fall slightly within the lower part of PS9 to a secondary trough (minimum value of 1.7‰ at 9.00 m), above which values again rise towards the top of PS9, with values above 3.0‰.

The lower part of PS10 occurs in the Upper NCC Cutting and can be traced across the Dudley area by the presence of a prominent hardground and bentonite (WHN10; Ray et al. 2011) at its base and an overlying succession containing multiple bentonite horizons. In order to access the entirety of PS10 two sections within the large Reef Knoll Quarry (Wren's Nest Hill) have been used, with the highly distinctive *Clematocrinus* Bed (see Ray & Thomas, 2007) used to precisely tie the sections together. Within PS10 isotopic values continue to rise with peak values (3.8‰) achieved within the lower 4.0 m of the parasequence. This peak corresponds to the upper peak of the Homerian CIE, above which values progressively fall throughout the remainder of the PS10 and the MWLF.

The transition from the Nodular Beds Member to the Upper Quarried Limestone Member takes place approximately 0.5 m below the Ripple Beds (a highly distinctive mega-rippled grainstone bed) (Davies *et al*. 2011). This distinctive bed marks the top of the measured section in the Reef Knoll Quarry and allows for correlation to Snake Pit Quarry (Mons Hill) where the entirety of PS11 can be accessed (Davies *et al*. 2011). Here PS11 broadly reflects a plateau in isotopic values with most values slightly above 2.0‰.

The boundary between PS11 and PS12 and the transition between the Upper Quarried Limestone Member (MWLF) and the Lower Elton Formation is faulted in Snake Pit Quarry. Accordingly, the stratigraphically overlapping Lion's Mouth Cavern section (Wren's Nest Hill) has been used to document this transition, with the widely traceable stromatoporoid pavement at the base of PS12 used to correlate between sections. In addition, as the boundary between PS11 and PS12 is considered to approximate to the Wenlock-Ludlow Series boundary (Blain et al. 2016), a 1.7 m overlap in stratigraphic position of isotope samples was made to demonstrate the correlation between the sections. Furthermore, the isotopic sampling of the entirety of the Lion's Mouth Cavern section was considered important as it has not previously been analysed for carbon isotopes and contains a high-resolution radioisotopic date (Cramer et al. 2012) (Figs. 3 and 5). Within the Lion's Mouth Cavern section, $\delta^{13}C_{carb}$ values in the Upper Quarried Limestone Member initially range from 2.2‰ to 1.9‰ (0.00 m to 1.68 m) and occur within the upper part of PS11. Above values fall markedly to 0.6‰ (2.71 m) within the lower part of PS12 (Passage Beds) and are considered to correspond to the end of the Homerian CIE. Values then recover slightly to a minor peak of 1.2‰, before falling again into the basal Lower Elton Formation (PS13) to a minimum value of 0.2‰.

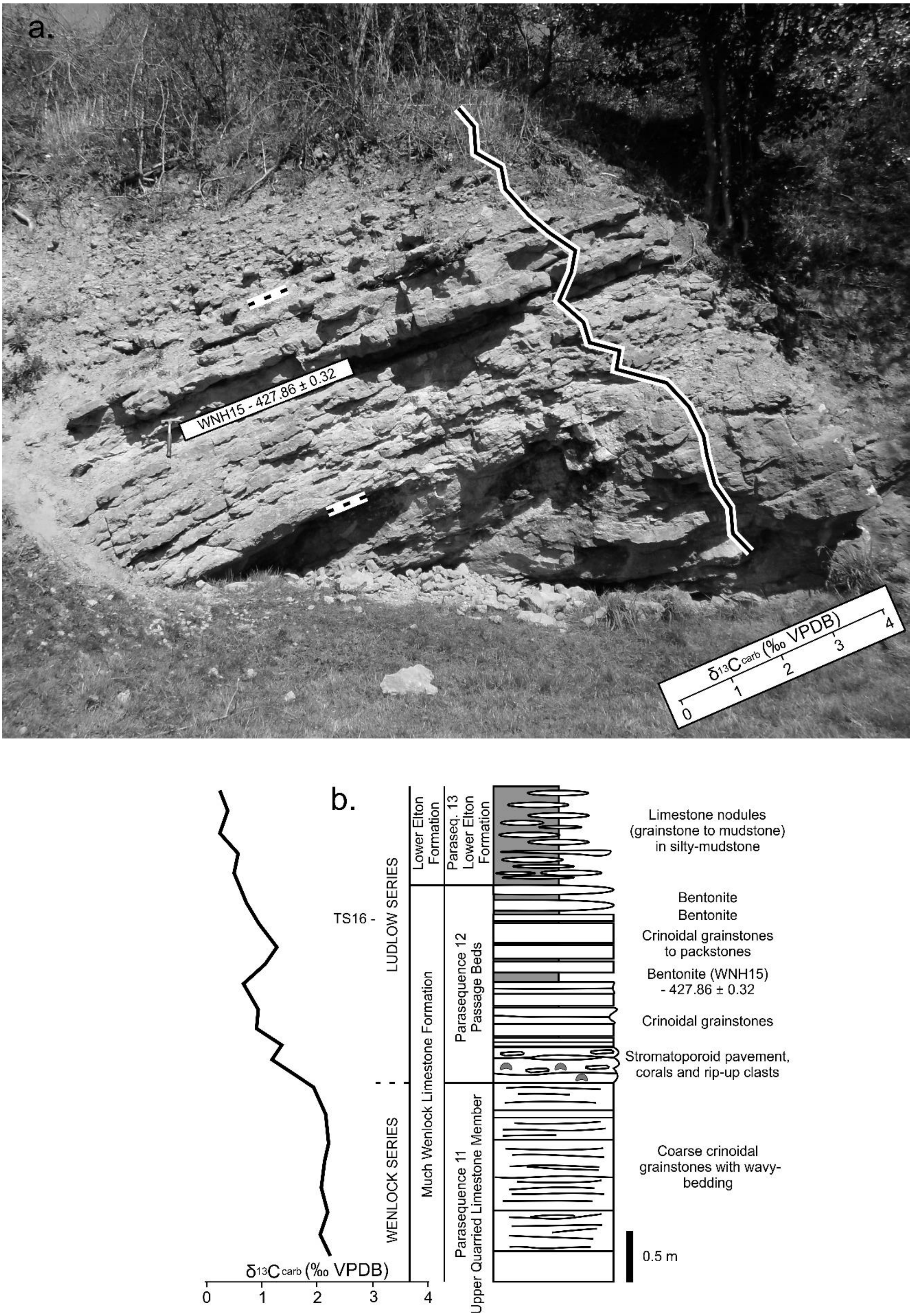

Figure 5. The carbon isotopic record across the Much Wenlock Limestone-Lower Elton

Formation boundary at Dudley. (a) The Lion's Mouth Cavern section and the carbon isotopic record. (b) Stratigraphic overview of the Lion's Mouth Cavern section.

4. A comparison of composite carbon isotope curves from Hereford-Worcestershire and the West Midlands

In a broad sense the Homerian CIE, as identified in both Hereford-Worcestershire (Storridge and Suckley) and West Midlands (Dudley) show rather similar features (Fig. 6), in that they identify a dual-peaked positive excursion that is chiefly confined to the MWLF, with peak values achieved near the bottom and top of the formation. However, in detail there are a number of notable differences, which can be stratigraphically located by the correlation of parasequences (Ray *et al*. 2013). For example, onset of the Homerian CIE in both sections takes place close to the Coalbrookdale-Much Wenlock Limestone formation boundary, but within the West Midlands a pronounced rise in values from 1‰ to 3‰, which may be taken at the onset of the CIE, occurs within the Basement Beds (PS0; uppermost Coalbrookdale Formation), while in Hereford-Worcestershire the same positive shift in values occurs within the basal Lower Quarried Limestone Member (PS1; basal MWLF). Above, both areas show a continued rise in carbon isotopic values within PS1 of the Lower Quarried Limestone Member, with the peak values achieved within PS2. However, while the position of the lower peak of the Homerian CIE is consistent with respect to the parasequence assignment, the absolute maximum values of the lower peak are 0.7‰ higher in the West Midlands area. A gradual decline in values from the Lower Quarried Limestone Member into the Nodular Beds Member is observed in both areas, but with the broad trough (minimum) in values occurring in PS7 in the West Midlands and around the PS9-PS10 boundary in Hereford-Worcestershire. Notably, the trough in values in the

West Midlands has an obvious equivalent within PS7 in Hereford-Worcestershire; the correlation of which is strongly supported by the immediately overlying bentonite correlation. Similarly, the main trough in values in Hereford-Worcestershire appears to be equivalent to a secondary trough in values within PS9 in the West Midlands, above which values increase to the upper peak of the Homerian CIE. The upper peak of the Homerian CIE occurs within PS10, but within the middle part of the parasequence in the West Midlands and near its top in Hereford-Worcestershire. In addition, the maximum isotope values associated with the upper peak are 0.8‰ higher in West Midlands. Finally, the decline in values towards the end of the CIE shows considerable similarities with the excursion ending within the Passage Beds (PS12).

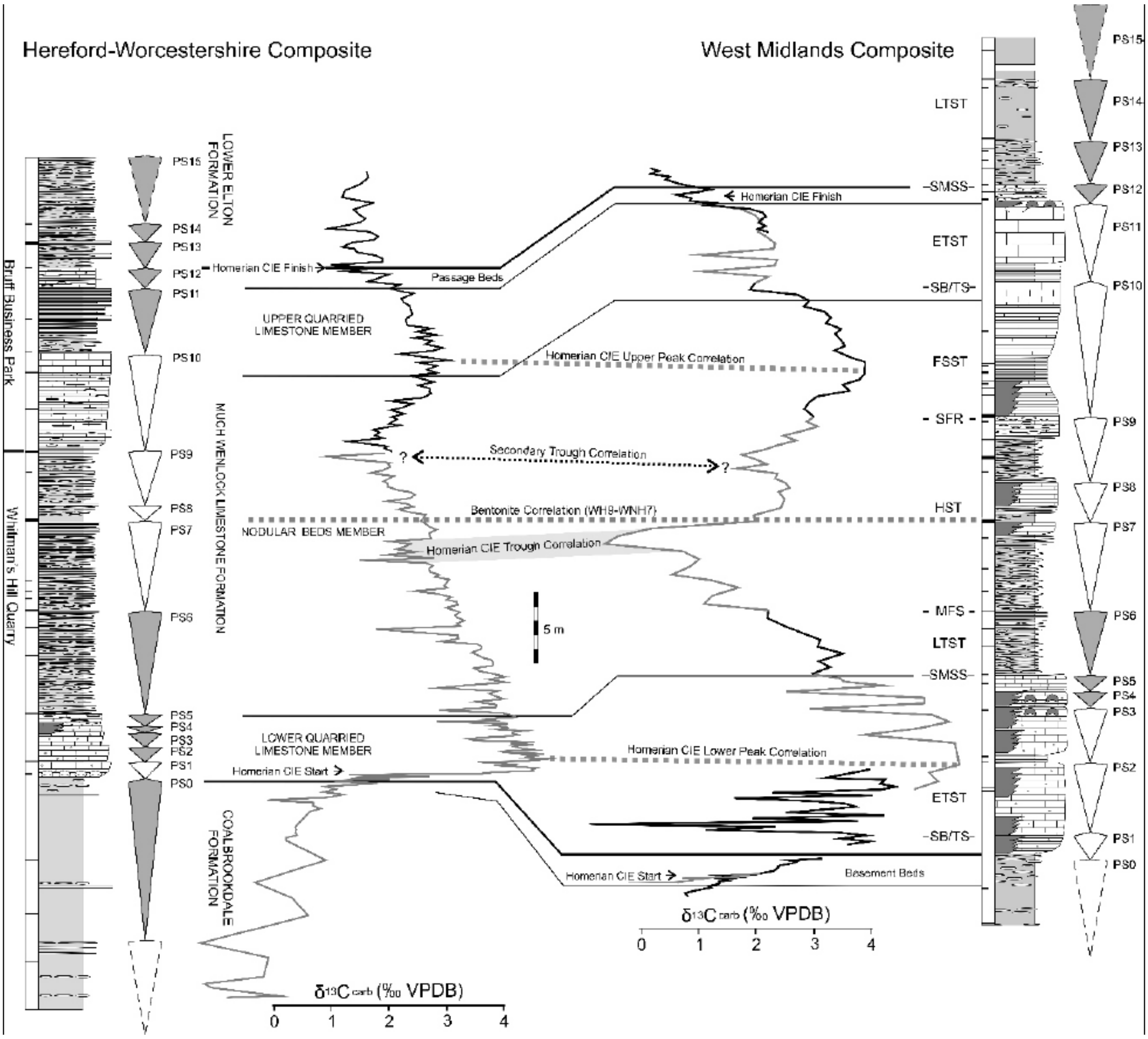

Figure 6. A comparison between the composite carbon isotopic curves derived from the Hereford-Worcestershire (Storridge and Suckley) and the West Midlands (Dudley) areas (see Fig. 2 for the key).

As outlined above, the Homerian CIE, as identified in both Hereford-Worcestershire and West Midlands show notable differences superimposed upon a common trend. The origin of such apparent differences in carbon isotopic trends may be interpretative (e.g. identifying the start and finish of a CIE), the impact of palaeobathymetry upon the carbon isotopic values, or primary and diagenetic rock mineralogy. Using the high-resolution stratigraphic framework outlined above we will investigate variation in palaeobathymetry across the study area and assess their impact upon carbon isotopic values. Mineralogy and diagenetic overprints are further qualitatively assessed in thin sections.

5. Facies, depositional environments and relative sea-level change

Interpretations of facies, depositional environments and relative sea-level change have been previously published for the Storridge, Suckley (Hereford-Worcestershire) and Dudley (West Midlands) areas (e.g. Butler, 1939; Phipps & Reeve, 1967; Oliver, 1981; Ratcliffe, 1988; Ratcliffe & Thomas, 1999; Ray & Thomas, 2007; Ray *et al*. 2010; Ray *et al*. 2013; Päßler *et al*. 2014; Jarochowska *et al*. 2018). Therefore, here we provide an overview with a focus upon those parts of the succession that show considerable regional variability and may consequently impact upon the local carbon isotopic signature (Figs. 2, 3, 6).

5.a. Coalbrookdale Formation

The Coalbrookdale Formation is more than 200 m thick within the platform interior (Cocks *et al*. 1992), though poor exposure typically restricts access to all but a few metres below the base of the MWLF. Across the platform interior the transition between the outer-shelfal silty-mudstones of the Coalbrookdale Formation and the inner-shelfal carbonates of the MWLF represents a major relative sea-level fall and sequence boundary of probable eustatic origin (see Johnson, 2006). However, in detail, a limestone-rich uppermost few metres to the Coalbrookdale Formation is only well-developed within the Dudley area (the Basement Beds), suggesting a slightly shallower depositional setting in this area, when compared to Whitman's Hill Quarry (Hereford-Worcestershire).

Thin section analysis of this interval further supports this interpretation of the uppermost Coalbrookdale Formation. At Whitman’s Hill Quarry thin sections (Figs. 2, 7) reveal mudstones with an admixture of silt-sized quartz grains and with lenses of bioclastic packstone to floatstone bounded by erosional surfaces (Fig. 7i). Near the very top of the formation layers and nodules of laminated, very well sorted, fine-grained peloidal grainstones with rare subplanar burrowing traces (Fig. 7j-k) are present. In addition, bioclasts are commonly encrusted by the problematicum *Allonema* (Fig. 7h).

Based upon these thin sections the Coalbrookdale Formation at Whitman's Hill Quarry is interpreted to have been deposited in an environment predominantly below the fair-weather wave base, but above the storm wave base, as indicated by episodes of erosion and reworking resulting in deposition of coquinas composed of poorly sorted, barely fragmented brachiopod shells. Intercalations of laminated peloidal grainstones with erosional bases in the uppermost part are here interpreted as produced by waning storm flows. Almost completely preserved lamination and sparse bioturbation indicate event deposition contrasting with the thorough bioturbation of the surrounding sediments.

By way of contrast the silty-mudstones of the Coalbrookdale Formation and overlying Basement Beds at Castle Mill Basin, West Midlands (Figs. 4, 7) contain crinoidal wacke- to packstones with grainstone nodules (Fig. 7a). Putative cyanobacteria *Rothpletzella* (Fig. 7d) and *Girvanella*, green algae *Rhabdoporella* (Fig. 7a) and *Dimorphosiphon* (Fig. 7c) are abundant. Common components include bryozoans (Fig. 7b), unidentified spherical fossils with very thin recrystallized shells (Fig. 7g), tentaculitids (Fig. 7f), trilobites, gastropods, phosphatic microfossils, and rare brachiopods. Finally, as with Whitman's Hill Quarry, bioclasts are commonly encrusted by the problematicum *Allonema* (Fig. 7b, e).

Based upon these thin sections the Coalbrookdale Formation at Castle Mill Basin is interpreted to have been deposited in a soft-bottom protected environment within the euphotic zone, oscillating near the fair-weather wave base, and therefore within a somewhat shallower setting than that for Whitman's Hill Quarry.

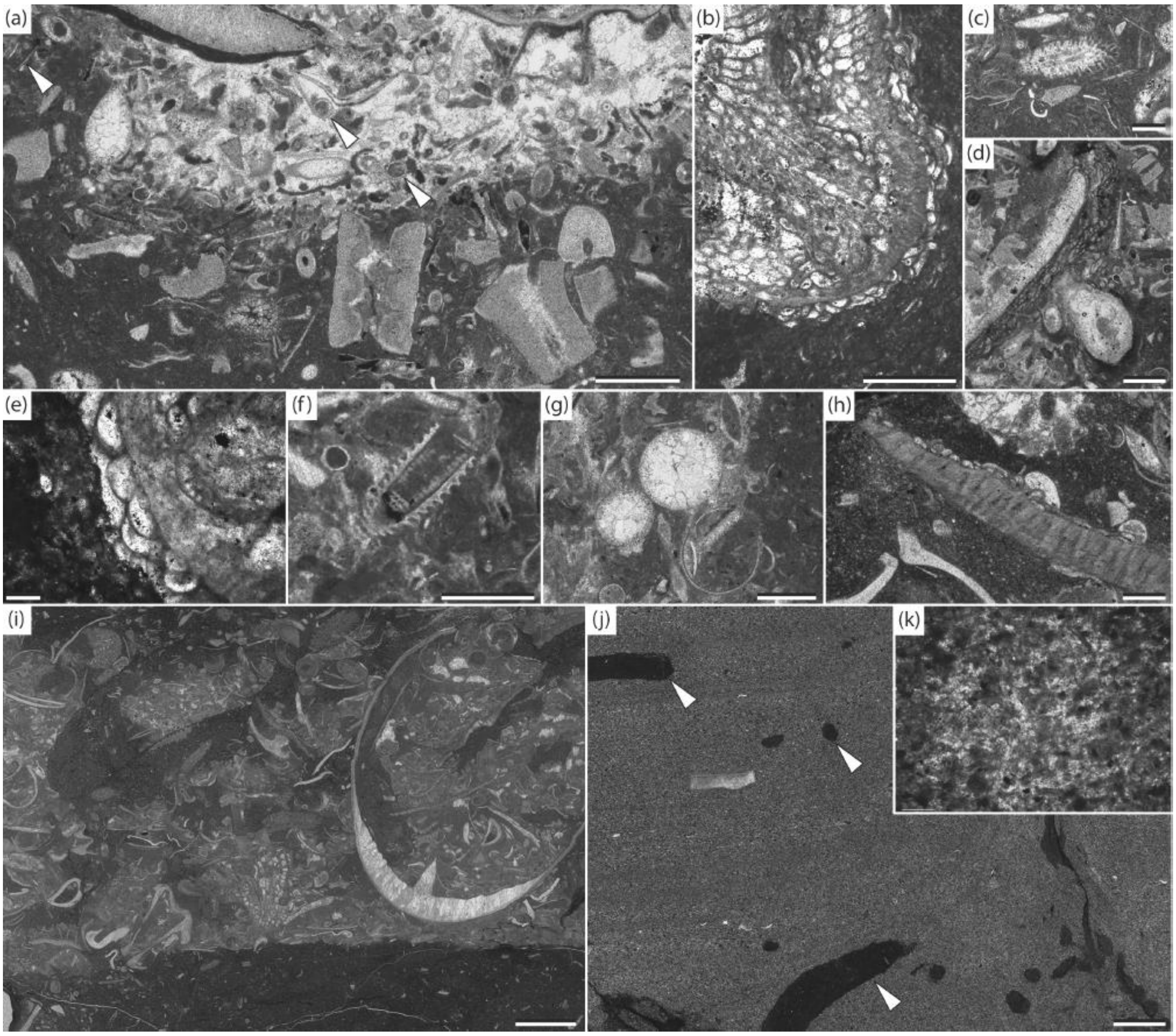

Figure 7. Microfacies of the uppermost part of the Coalbrookdale Formation; see figures 2 and 3 for thin section (TS) locations). (a) Transition from crinoidal wacke- to grainstone; arrows point to *Rhabdoporella*, thin section 2 (TS2), Castle Mill Basin,

scale bar 1 mm. (b) Bryozoan encrusted with *Allonema*, thin section 1 (TS1), Castle Mill Basin, scale bar 500 µm. (c) Calcareous green alga *Dimorphosiphon*?, thin section 1 (TS1), Castle Mill Basin, scale bar 750 µm. (d) Crinoidal packstone with recrystallized shells encrusted with *Rothpletzella*, thin section 2 (TS2), Castle Mill Basin, scale bar 100 µm. (e) Close-up of *Allonema* in (b), scale bar 200 µm. (f) Tentaculite, thin section 2 (TS2), Castle Mill Basin, scale bar 1 mm. (g) Spherical unidentified components with thin recrystallized walls, thin section 3 (TS3), Castle Mill Basin, scale bar 1 mm. (h) Brachiopod shell encrusted with *Allonema*, thin section 4 (TS4), Whitman's Hill, scale bar 500 µm. (i) Bioclastic pack- to floatstone over an erosional boundary cutting into a poorly fossiliferous mudstone, thin section 4 (TS4), Whitman's Hill, scale bar 3 mm. (j) Laminated peloidal grainstone with sparse bioturbations (arrows), thin section 5 (TS5), Whitman's Hill, scale bar 3 mm. (k) Close-up of the peloidal grainstone in (j), scale bar 200 µm.

5.b. Lower Quarried Limestone Member of the Much Wenlock Limestone Formation

The Lower Quarried Limestone Member of the MWLF is regionally variable in thickness and ranges from as little as 4.3 m at Whitman's Hill Quarry to 8.2 m at Bruff Business Park, and to between 9.8 m and 16.2 m in the West Midlands (Ray *et al*. 2010; Ray *et al*. 2013). An important factor in determining the thickness of any one section is the presence of reefal masses, with greater thicknesses attributed to variations in compaction and lithification caused by their presence (Ratcliffe, 1988). However, regional variations in the bedded lithology are present and indicate a thinning and eventual loss of these limestones at the transition with the exterior part of the platform (see Ratcliffe & Thomas, 1999; Ray *et al*. 2010; Fry *et al*. 2017). In detail the bedded parts of the succession can be divided into five parasequences (PS1 to 5) with the top of PS1 corresponding to a combined sequence boundary and transgressive surface (Ray *et al*. 2013). Above, relative sea-level is interpreted to gradually increase at Whitman's Hill Quarry, while within the West Midlands relative sea-level fell throughout much of the remainder of the member, reflecting differing local responses of carbonate production to sea-level rise within the early transgressive systems tract (Figs. 2, 3, 6).

The boundary between the Coalbrookdale Formation and Lower Quarried Limestone Member at Whitman's Hill Quarry represents a major relative sea-level fall (Fig. 2). PS1 differs from the overlying strata of the member: its base is formed by mudstone with an admixture of silt-sized quartz with rare, thoroughly fragmented and partly pyritized brachiopods, ostracods, bryozoans, and trilobites. Within this matrix, large in situ favositid corals can be traced to Penny Hill Quarry (~13 km north of Whitman's Hill Quarry) (Ray *et al*. 2013). The top of this parasequence is visible in the field as an iron oxide-stained, scoured surface marking erosion at a sequence boundary. It consists of a moderately sorted crinoidal grainstone layer with cortoids (Fig. 8b), reworked lithoclasts, and porostromate oncoids (Fig. 8d-e). Above, the parasequences of the early transgressive systems tract are formed of two facies types. The first is oncoidal floatstones with moderately diverse benthic fauna, including gastropods, rugose corals, crinoids, bryozoans, and ostracods (Fig. 8a). Most bioclasts are encrusted with both spongio- and porostromate problematica (Fig. 8c), e.g. *Girvanella*. The matrix is clotted and peloidal, suggestive of microbially precipitated micrite. This interval also contains reefs, not examined here, but characterized previously by Penn (1971) and Päßler *et al*. (2014). The second and stratigraphically higher facies is mud- to wackestones with rare complete rugose corals in life positions. This interval is partly dolomitic, as indicated by the lack of reaction with acetic acid (Jarochowska *et al*. 2017), but neither obvious dolomitization affecting rock texture nor microbial structures typical for primary dolomite have been observed in thin sections or macroscopically. This allows the possibility that dolomite was present in the fine fraction, as reported from other carbon isotope excursion intervals (Kozłowski & Sobień, 2012; Frýda & Frýdova, 2016). Oncoids are absent and putative cyanobacteria are less common, typically in association with the non-microbial problematicum *Allonema* (Fig. 8f-g), which also encrusts most available substrates. The matrix is bioturbated, giving the rock amalgamated appearance. Benthic fauna is fragmented and consists of gastropods, ostracods, trilobites, and rare crinoids.

Based upon the microfacies descriptions the base of PS1 was deposited between storm and fair-weather wave base. The scarcity of benthic fauna and lack of green algae indicate either restricted conditions or relatively deep environment. The high degree of fragmentation is suggestive of long transport, supporting the latter explanation. On the other hand, the very large size and high degree of colony integration in favositids are commonly taken as indicator of their photosymbiotic mode of growth (e.g. Stanley & Lipps, 2011) and large colonies might indicate position within the photic zone. The remainder of PS1 records a rapid lowering of the erosional base, with the scoured surface at the top of the parasequence indicating submarine winnowing. The iron oxide mineralization of this surface is likely derived from the overlying bentonite (WH4 of Ray *et al*. 2013) that was preserved during the onset of relative sea-level rise associated with the proceeding parasequence.

The presence of green algae within much of the overlying Lower Quarried Limestone Member indicates deposition within the euphotic zone (Päßler *et al*. 2014). All oncoids observed are small, smooth-surfaced, and spherical to subspherical (Type

A oncoids of Ratcliffe, 1988) and indicate deposition within fair-weather wave base. Only the topmost part of the member was deposited below the fair-weather wave base and the euphotic zone (Päßler *et al*. 2014), with the amalgamation through burrowing organisms suggestive of low depositional rates at this time.

At Dudley the microfacies of the Lower Quarried Limestone Member have been documented in detail (Ratcliffe, 1988; Ratcliffe & Thomas, 1999), with three microfacies attributed to the bedded part of the succession (peloidal packstones; skeletal packstones and wackestones; loosely packed skeletal wackestones) and three attributed to reefal masses and their immediate surroundings (coralline framestones (= graticulacean algae); crinoidal grainstones; algal micrites). More generally the common occurrence of oncoids and green algae indicates that deposition took place mostly within the euphotic zone. With respect to relative sea-level change and depositional energy much insight has been gained from the analysis of oncoid morphology. Broadly, the oncoids range from large (< 70 mm), highly irregular branched forms to small (5–10 mm) subspherical forms, with the degree of rolling during formation responsible for differences in morphology. Using a simple classification of oncoid morphology (types A, B and C), Ratcliffe (1988) demonstrated that across the West Midlands there is a vertical transition from irregular Type C oncoids to subspherical Type A forms. Such an arrangement indicates an overall increase in depositional energy from an environment close to storm wave base, being characterised by low energy with little turbulence (Type C oncoids), to an environment within fair-weather wave base, with Type A oncoids requiring constant but gentle rolling (Ratcliffe, 1988).

Based upon a regional comparison of the environmental changes within the uppermost Coalbrookdale Formation and Lower Quarried Limestone Member it is apparent that as sea-level fell across the platform interior the position of the highest depositional energy shifted from the West Midlands (the Basement Beds) to Hereford-Worcestershire and Whitman’s Hill Quarry (basal Lower Quarried Limestone Member). This shift resulted in the dissipation of wave energy within formerly low energy deeper water areas (i.e. Whitman’s Hill Quarry), and the establishment of a sheltered lagoon across the West Midlands. Above the sequence boundary the onset of sea-level rise (early transgressive systems tract) resulted in an eventual return of high-energy deposition to the West Midlands (Type A oncoids of the higher part of the Lower Quarried Limestone Member), while at Whitman’s Hill Quarry deposition returned to below fair-weather wave base and the euphotic zone. It is of note that high-energy deposition within the West Midlands during parasequences 4 and 5 most likely reflected the onset of relative sea-level rise, as inferred by features such as parasequence thickness and lithological variability (Ray *et al*. 2010).

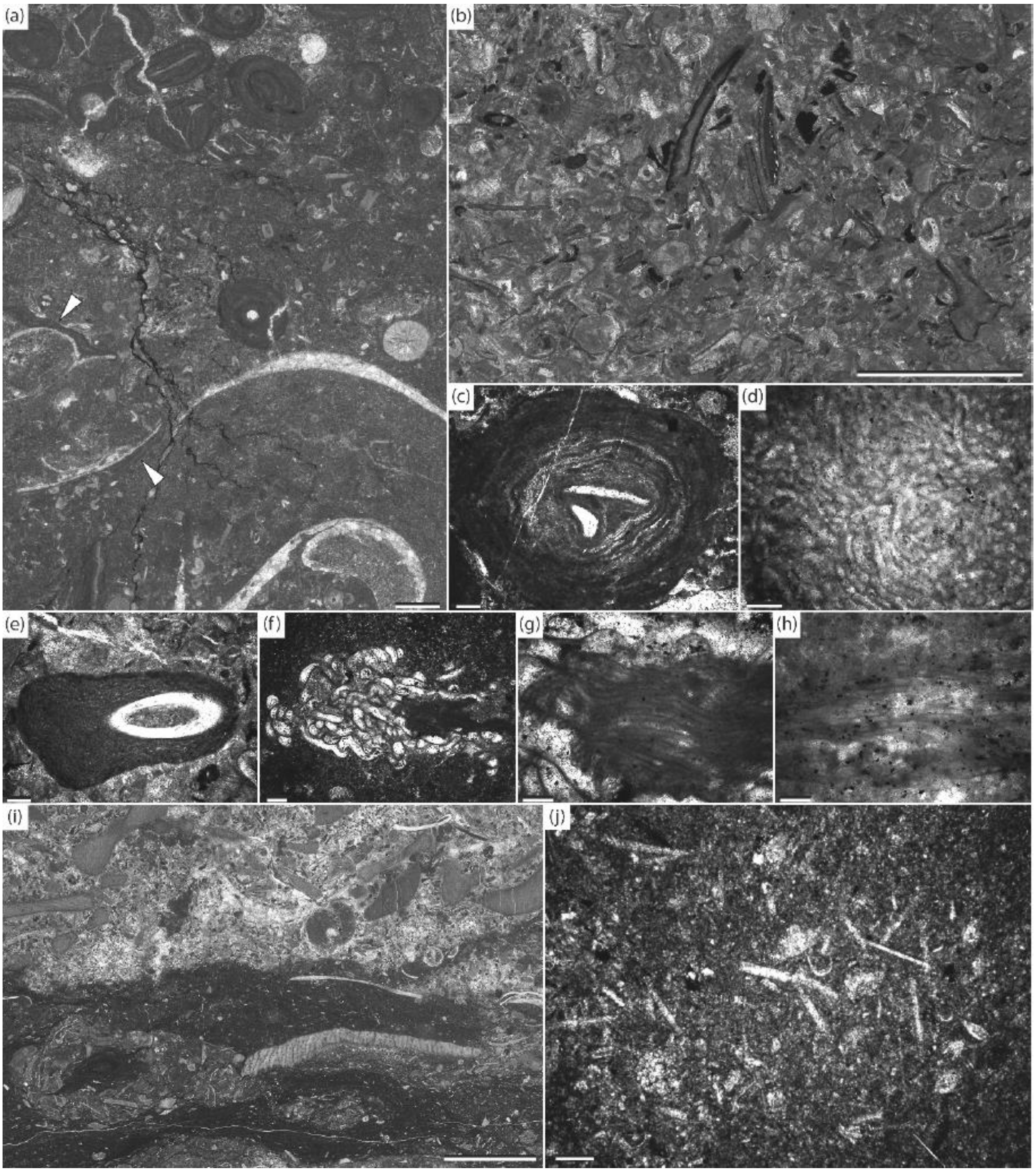

Figure 8. Microfacies of the Lower Quarried Limestone (a-g) and Nodular Beds (h-j) members; see figures 2 and 3. (a) Oncoid-gastropod floatstone, arrows show algal coating on recrystallized gastropod shell, thin section 7 (TS7), Whitman's Hill, scale bar 2 mm. (b) Crinoidal pack- to grainstone with cortoids, thin section 6 (TS6), Whitman's Hill, scale bar 4 mm. (c) Oncoid formed by probable *Girvanella*, thin section 7 (TS7), Whitman's Hill, scale bar 500 μm. (d) Close-up of a porostromate

problematicum forming an oncoid, thin section 6 (TS6), Whitman's Hill, scale bar 200 μm. (e) Truncated oncoid formed by a porostromate problematicum, thin section 6 (TS6), Whitman's Hill, scale bar 500 μm. (f) Aggregation of *Girvanella* and *Allonema* floating in the matrix, thin section 8 (TS8), Whitman's Hill, scale bar 500 μm. (g) Close-up of *Girvanella* in (f), scale bar 200 μm. (h) *Girvanella* floating in a grainstone, thin section 9 (TS9), Whitman's Hill, scale bar 500 μm. (i) Contact between crinoidal bioturbated wacke- to packstone and crinoidal grainstone with peloids, thin section 11 (TS11), Bruff Business Park, scale bar 4 mm. (j) Sponge spicules in a wackestone matrix, thin section 10 (TS10), Bruff Business Park, scale bar 500 μm.

5.c. Nodular Beds Member of the Much Wenlock Limestone Formation

The Nodular Beds Member of the MWLF increases in thickness from 23.0 m within Hereford-Worcestershire (Bruff Business Park) to 27.8-31.0 m within the West Midlands. The member consists of nodular and bedded limestones separated by silty mudstones of a similar thickness. In terms of relative sea-level change, the member begins with a marked sea-level rise (late transgressive systems tract) of probable eustatic origin (transgression 5a of Johnson, 2006), above this sea-level falls, slowly at first and then more rapidly within the upper part of the member (highstand and falling stage systems tracts) (Ray *et al*. 2010, 2013). Based upon the common occurrence of reefs and skeletal limestones, the succession in the West Midlands appears to be developed within a somewhat shallower setting than that within Hereford-Worcestershire. In particular, at Dudley skeletal limestones and reefs return within PS7, above which PS8 is particularly notable as a massively bedded interval consisting of packstones and grainstones with reefal masses (i.e. a high-energy setting within the euphotic zone). The onset of this reefal facies is observable across the West Midlands (Ray & Thomas, 2007; Ray et al. 2010) and marks the beginning of pronounced shallowing, that culminates in the wave-rippled grainstone beds and the uppermost Nodular Beds and Upper Quarried Limestone member.

At Whitman's Hill Quarry and Bruff Business Park the beds of the Nodular Beds Member are partly amalgamated and obliterated by formation of nodules. The lower part of the member (PS6) is a partly dolomitized mudstone with crinoids, small, solitary rugose corals, and a high content of clay and siliciclastic mud. Stratigraphically higher in the member (PS8 and 9) the proportion of clay is lower and nodularity is more pronounced. Nodules are surrounded by silty mudstones with dissolution seams and formed by very fine-grained bioclastic wackestone with crinoids and abundant sponge spicules (Fig. 8j). The contact with the uppermost parasequence (PS10) (Fig. 8i) shows an abrupt shift to purer carbonates formed by wacke- to packstones with grainstone nodules containing *Dimorphosiphon*-like green algae.

Based upon the microfacies descriptions the basal parasequence (PS6) of the Nodular Beds Member was deposited near the storm wave base at very low rates of carbonate production and is considered characteristic of the late transgressive systems tract. The top of PS9 is reflective of a general shallowing trend (highstand systems tract) with increasing abundance and diversity of benthic fauna. However, the absence of photic zone indicators and high abundance of sponges indicates relatively deep environment below storm wave base. Finally, the base of PS10 represents the surface of forced regression and marks an abrupt shallowing to the euphotic zone. In addition, the increasing proportion of grainstones in this unit indicates deposition initially near and subsequently above the fair-weather wave base (falling stage systems tract).

Based upon a regional comparison of the Nodular Beds Member it is clear that a high-energy setting within the euphotic zone was achieved much earlier within the West Midlands (PS7), while within Hereford-Worcestershire such a setting is only achieved by PS10. Thus, for a significant portion of the deposition of the Nodular Beds Member the West Midlands represented a potentially restricted patch-reef setting, while Hereford-Worcestershire reflected the relatively open waters of the margin of the platform interior.

5.d. Upper Quarried Limestone Member of the Much Wenlock Limestone Formation

The thickness of the Upper Quarried Limestone Member varies from 7.51 m (including the Passage Beds; PS12) at Bruff Business Park to between 8.6 m to 10.2 m across the West Midlands (Aldridge *et al*. 2000). Across the study area the member begins within thickly bedded to massive grainstones that develop towards the top of PS10. The top of PS10 is a combined sequence boundary and transgressive surface and represents the peak of a major relative sea-level fall of probable eustatic origin (see Johnson, 2006). Above, the succession is considerably more variable in lithology and thickness (PS11 and PS12). Such variations reflect the onset of regional sea-level rise (early transgressive systems tract), differences in palaeobathymetry and the localised development of grainstone shoals (Ray *et al*., 2010, 2013; Blain *et al*. 2016). Finally, the onset of rapid regional sea-level rise (late transgressive systems tract) replaces the inner-shelfal carbonates of the MWLF with the outer-shelfal silty mudstones of the Lower Elton Formation. We here confine our descriptions to the successions at Bruff Business Park (Suckley) and Lion’s Mouth Cavern (Dudley) (Figs. 2, 5, 6).

Microfacies analysis at the Bruff Business Park identifies the massive nodular limestones that develop towards the top of PS10 as consisting of a poorly sorted crinoidal grainstone with diverse ostracods, bryozoans, brachiopods and echinoderms (Fig. 9a). Above PS11 consists of evenly bedded silty mudstones intercalating with limestone nodules and thin limestone beds. The mudstones are moderately bioturbated and have a diverse ostracod and bryozoan fauna. Grainstone beds formed by well-sorted crinoids and ostracods have been found cutting erosionally into the mudstones (Fig. 9c). Limestone beds show planar lamination formed by very well sorted, very fine sand fraction peloidal grainstones with abundant organic-walled fossils – scolecodonts and chitinozoans, and *Planolites*-like burrows (Fig. 9b). The Passage Beds equivalent occurs in parasequence 12 and may be distinguished by a slightly more nodular appearance than the overlying Lower Elton Formation (included in the Lower Elton Formation of Ray *et al*. 2013), but otherwise is broadly similar. This unit is distinguished by a shift to fine-grained sedimentation and the formation of silty nodular mudstones with sparse bioturbation. Lenses of bioclastic float- to rudstones with diverse bryozoans, crinoids, brachiopods, trilobites, ostracods, and halysitid corals (Fig. 9d) appear partially reworked by bioturbation.

In contrast to the Bruff Business Park section, at Lion’s Mouth Cavern (Dudley, West Midlands) PS11 is developed as coarse thick-bedded crinoidal grainstones. Above, the Passage Beds (PS12) begin with a very coarse grainstone with shale and limestone rip-up clasts, stromatoporoids and corals both rolled and in situ, and very coarse crinoid ossicles. This unit is followed by thin-bedded, amalgamated crinoidal rudstones grading into grainstones and fine-grained, well-sorted packstones with quartz grains in the fine sand size fraction. In the upper part numerous crinoid ossicles are phosphatized (Fig. 9e-f).

Based upon the microfacies descriptions the variability in depositional environment and relative sea-level within the Upper Quarried Limestone Member and immediately overlying Lower Elton Formation may be assessed. At Bruff Business Park the initial grainstone succession at the top of PS10 is interpreted as deposition in a shoal environment, i.e. above the fair-weather wave base. Above PS11 is representative of relative sea-level rise and the onset of the early transgressive systems tract. Here deposition occurred in a soft-bottom environment. Low faunal abundance and the lack of photic zone indicators point to a relatively deep environment. Distal tempestites formed as laminated grainstones, identical to those in the upper part of the Coalbrookdale Formation, point to deposition above the storm wave base. Within the overlying Passage Beds and basal Lower Elton Formation relative seal-level continued to rise. A low diversity of benthic fauna indicates deposition in a relatively deep environment, but above the storm wave base, as indicated by storm beds bringing shallow-water material. In addition, limited bioturbation might suggest comparatively high depositional rates or limited oxygen availability.

By contrast PS11 at Lion's Mouth Cavern is reflective of deposition in a high-energy shoal environment and indicates continued relative sea-level fall within the Dudley area. It is not until the overlying Passage Beds (PS 12) that relative sea-level notably rises. Here the Passage Beds reflect oscillation near the fair-weather wave base, and the phosphatization of bioclasts is interpreted to represent sediment-starvation as sea-level increased.

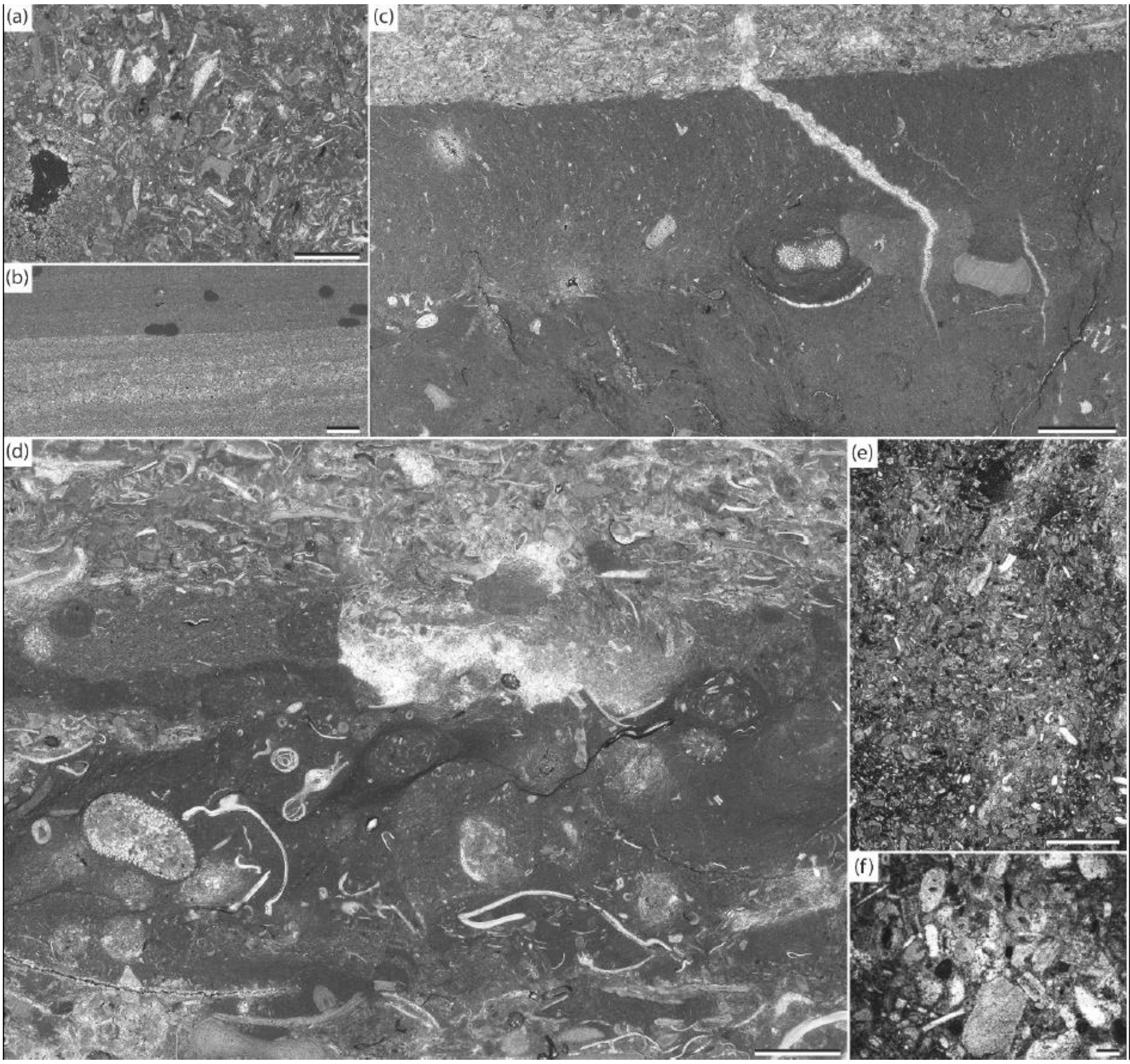

Figure 9. Microfacies of the Upper Quarried Limestone Member (a-c, e-f) and Lower Elton Formation (d); see figures 2 and 4. (a) Partly dolomitized crinoidal packstone, sample 12 (TS12), Bruff Business Park, scale bar 3 mm. (b) Laminated peloidal grainstone with *Planolites*-like bioturbations, sample 14 (TS14), Bruff Business Park, scale bar 3 mm. (c) Erosional contact between bioturbated bioclastic wackestone and crinoidal grainstone, sample 13 (TS13), Bruff Business Park, scale bar 3 mm. (d) Erosional contact between bioturbated bioclastic float- to rudstone and crinoidal pack- to grainstone, sample 15 (TS15), Bruff Business Park, scale bar 3.5 mm. (e)

Bioturbated crinoidal packstone with phosphatized crinoids, sample 16 (TS16), Lion's Mouth Cavern, scale bar 2.5 mm. (f) Close-up of (e), scale bar 500 μm.

Based upon a regional comparison of the Upper Quarried Limestone Member, it is apparent that with the onset of the early transgressive systems tract the relatively deeper-water carbonates of Hereford-Worcestershire failed to keep pace with sea-level rise, while those in the West Midlands initially outpaced sea-level rise. This resulted in markedly different depositional environments cross PS11 and PS12, above which the increased rate of sea-level rise (late transgressive systems tract) regionally replaced the inner-shelfal carbonates of the MWLF with the outer-shelfal silty-mudstones of the Lower Elton Formation.

6. The impact of depositional environment upon the Homerian Carbon Isotope Excursion

The subdivision and correlation of the Much Wenlock Limestone Formation and the immediately under- and overlying formations by parasequences allows for the investigation of age synchronous, but depositionally divergent environments (Figs. 2, 3, 6). Based upon the analysis of microfacies herein these differences have been qualitatively assessed in terms of their position with respect to storm and fair-weather base and the euphotic zone, thereby allowing for a better understanding of the environmental differences between sections. These depositional differences can now be compared with differences in the carbon isotopic record.

At the broadest scale it is apparent that for any given time interval the shallowest depositional setting is consistently developed within the West Midlands. This observation is most apparent during episodes of rapid (eustatic) sea-level change where higher-energy (and shallower) microfacies occur earlier during sea-level fall and persist later during sea-level rise. In terms of the effect upon carbon isotopic values it has been well documented that lighter $\delta^{13}C_{carb}$ values are recorded from more distal settings and heavier values from shallower settings, and this relationship has been demonstrated in near-age equivalent successions on Avalonia (Blain *et al*. 2016), Baltica (Jarochowska & Munnecke, 2015), and Perunica (Frýda & Frýdova, 2016). Based upon the maximum $\delta^{13}C_{carb}$ values for the lower and upper peaks of the Homerian CIE this also holds true for the MWLF with values in the West Midlands 0.7‰ and 0.8‰ higher than in Hereford-Worcestershire. The likely range of isotopic values within the carbonates of the Midland Platform may be established for the lower peak of the Homerian CIE, with values ranging from as low as 2.8‰ (Fry *et al*. 2017) for the most distal extreme of the carbonate deposition (Farley Member of the Coalbrookdale Formation at Eaton Track near Much Wenlock) to 5.5‰ for the most proximal setting at Dudley (i.e. a difference of 2.7‰).

At the scale of members and parasequences the effect of depositional environment and paleobathymetry upon carbon isotopic values can also be observed. These differences are most conspicuous within the Nodular Beds Member, where there is a regional difference between the position of the broad trough in values which separates the dual peaks of the Homerian CIE. In particular, within the West Midlands the broad minimum in values and turnaround to rising values occurs in PS7, while within Hereford-Worcestershire this occurs around the PS9-PS10 boundary (Fig. 6). From the perspective of paleobathymetry change, within the West Midlands the upper part of PS7 corresponds to the onset of reef development and the beginning of a pronounced shallowing, while within Hereford-Worcestershire a relatively deep environment below storm wave base and the euphotic zone persists until the base of

PS10, after which pronounced shallowing begins. Thus, the broad minimum in isotopic values and the turnaround to rising values appears to mirror the onset of pronounced shallowing within both areas. One possible interpretation of the stratigraphic off-set between troughs could be a mis-correlation of parasequences; which seems unlikely given the additional bentonite correlation within this critical interval. Moreover, superimposed upon the broad carbon isotopic trends of both areas are lesser troughs in values which appear to represent age equivalent isotopic events or local petrographic variations (Fig. 6). However, no support for the effect of diagenetic alterations or admixture of detrital minerals that might have shifted the isotopic values (see e.g. Kozłowski & Sobień, 2012) has been observed in thin sections. A strong diagenetic overprint on the isotopic values can be excluded based on the lack of relationship between $\delta^{18}O_{carb}$ and $\delta^{13}C_{carb}$ values (Supplementary Material). Accordingly, regional differences in the rate of paleobathymetric change and nature of the associated carbonates appear to control and off-set the broad trend in isotopic values, while shorter-term events are observable across the study areas.

Within the upper MWLF there is approximate synchronicity between the areas with respect to the position of the upper peak of the Homerian CIE. However, while the upper peak occurs in both areas within PS10, its position within the parasequence does differ. In particular, peak values occur in the lower half of PS10 in the West Midlands and the upper half PS10 in Hereford-Worcestershire. As previously this off-set may also be the result of differing paleobathymetries upon isotopic values, but given the general upward shallowing nature of each parasequence and the similarly rapid fall in sea-level observed across the region this explanation seems less apparent. Thus, an alternative explanation might be that the intra-parasequence off-set of the peak values may reflect variable sedimentation rates and or minor regional diachronism. This view is additionally supported by the correlation of a bentonite within PS10 between Dudley and Wenlock Edge (Ray et al. 2011). As with the position of the isotopic peak, the bentonite horizon occurs lower in the parasequence at Dudley and at a relatively higher position towards the platform margin at Wenlock Edge. Irrespective of the cause, such minor differences do highlight the limit of the regional stratigraphic resolution and question significance of minor off-sets in the start and finish of the Homerian CIE highlighted herein.

Lastly, our ability to clearly identify the end of the Homerian CIE is of particular significance owing to its close proximity to the Wenlock-Ludlow boundary. Based upon the correlation of parasequences with the Gorstian GSSP (base Ludlow Series) at Ludlow (Shropshire) (Fig. 1b) (Melchin *et al*. 2012; Blain *et al*. 2016; Fry *et al.* 2018) this boundary corresponds to the PS11-PS12 boundary (the Much Wenlock Limestone-Lower Elton Formation boundary at Ludlow). Accordingly, the carbon isotopic records within the West Midlands and Hereford-Worcestershire would argue for the end of the Homerian CIE within the very earliest Ludlow (intra-PS12). However, the end of the Homerian CIE is far from clear within the Ludlow area (Fry *et al.* 2018) and this lack of clarity has been linked to platform margin depositional setting of the Ludlow area (Blain *et al*. 2016). In particular, within deeper-water settings the environmental difference between the latest Wenlock limestones of the MWLF (PS11) and the shales and limestones of the lowest Lower Elton Formation (PS12) becomes less marked and this is reflected by less variability within carbon isotopic record; thereby making the accurate establishment of the end of the CIE difficult. Conversely, within the platform interior the end of the Homerian CIE coincides with a marked sea-level rise and equally marked environmental change, which may have the effect of reducing carbon isotopic values and bringing to an end the Homerian CIE. Thus, the end of the Homerian CIE upon the Midland Platform may be partly reflective of local environmental changes, rather than global change within the carbon cycle. Furthermore, it is clear from this study that the variability of platform carbonates in response to sea-level has a significant impact upon the carbon isotopic record and this impact can only be understood by a careful analysis of depositional environment and paleobathymetry.

7. Conclusions

New $\delta^{13}C_{carb}$ and microfacies data from Hereford-Worcestershire (Storridge and Suckley) and the West Midlands (Castle Hill, Mons Hill and Wren's Nest Hill) allow for a detailed examination of variations in the Homerian CIE and depositional environment within the Much Wenlock Limestone Formation of the interior of the Midland Platform. The main conclusions are summarised below:

1. The entirety of the dual-peaked Homerian CIE is recognised for the first time with the Much Wenlock Limestone Formation of Hereford-Worcestershire and allows for a detailed comparison of new carbon isotope data from the West Midlands area using the sequence stratigraphic and bentonite correlation framework of Ray *et al*. (2013).
2. Thin section descriptions and microfacies analysis confirm the regional differences in relative sea-level change identified by Ray *et al*. (2013). In particular, the Much Wenlock Limestone Formation of West Midlands is developed within a somewhat shallower platform interior setting than that seen in Hereford-Worcestershire. This is most apparent during episodes of rapid (eustatic) sea-level change where higher-energy (and shallower) microfacies occur earlier during sea-level fall and persist later during sea-level rise.

3. Based upon the maximum $\delta^{13}C_{carb}$ values for the lower and upper peaks of the Homerian CIE the shallower depositional setting of the West Midlands is associated with values that are 0.7‰ and 0.8‰ higher than in Hereford-Worcestershire. Thus, lighter $\delta^{13}C_{carb}$ values are recorded from more distal settings and heavier values from shallower settings.
4. At the scale of members and parasequences the effect of depositional environment upon carbon isotopic values has been observed. In particular, there is a clear off-set in the position of the trough in isotopic values between the peaks of the Homerian CIE. This offset can be attributed to notably shallower parts of the succession within the West Midlands area. It appears to reflect differences in relative sea-level change and carbonate production rates. Furthermore, it may be influenced by rock mineralogy and the corresponding $\delta^{13}C$ fractionation, with higher values in shallower settings due to higher proportions of dolomite or aragonite.
5. Local differences in carbon isotopic values complicate their use as a means of high-resolution correlation. However, from this study it is clear that a careful analysis of the depositional environment and paleobathymetry can account for these differences and thereby improve our utilisation of this stratigraphic tool.

Acknowledgements

The authors thank Herefordshire and Worcestershire Earth Heritage Trust for access to Whitman's Hill Quarry and John Roberts-Powell for access to Bruff Business Park. We would also like to thank Dudley Canal and Tunnel Trust for providing access to the Castle Mill Basin sections and Dudley MBC for access to the sections within Wren's Nest National Nature Reserve. We thank B. Leipner-Mata for help in producing thin sections. The paper benefited from reviews by Jiri Frýda and two anonymous referees that significantly improved the manuscript. EJ and AM were supported by Deutsche Forschungsgemeinschaft (grant no. Mu 2352/3 to A. Munnecke).

Declaration of Interests. None

References

ALDRIDGE, R. J., SIVETER, DAVID J., SIVETER, DEREK J., LANE, D., PALMER, D. C. & WOODCOCK, N. H. 2000. *British Silurian stratigraphy*, xviii. Peterborough: Geological Conservation Review Series, Joint Nature Conservation Committee, 542 pp.

BASSETT, M. G., BLUCK, B. J., CAVE, R., HOLLAND, C. H. & LAWSON, J. D. 1992. Silurian. In *Atlas of Palaeogeography and Lithofacies* (eds. J. C. W. Cope, J. K. Ingham & P. F. Rawson), pp. 37-57. Geological Society, London Memoir 13.

BERGSTRÖM, S. M., LEHNERT, O., CALNER, M. & JOACHIMSKI, M. M. 2012. A new upper Middle Ordovician–Lower Silurian drillcore standard succession from Borenshult in Östergötland, southern Sweden: 2. Significance of $\delta^{13}C$ chemostratigraphy, *GFF* **134** (1), 39-63.

BLAIN J. A., RAY, D. C. & WHEELEY, J. R. 2016. Carbon isotope ($\delta^{13}C_{carb}$) and facies variability at the Wenlock-Ludlow boundary (Silurian) of the Midland Platform, UK. *Canadian Journal of Earth Sciences* **53** (7), 725-730.

BUGGISCH, W. & MANN, U. 2004. Carbon isotope stratigraphy of Lochkovian to Eifelian limestones from the Devonian of central and southern Europe. *International Journal of Earth Sciences (Geol Rundsch)* **93**, 521-544.

BUTLER, A. J. 1939. The stratigraphy of the Wenlock Limestone at Dudley. *Quarterly Journal of the Geological Society of London* **95**, 34-74.

COCKS, L. R. M., HOLLAND, C. H. & RICKARDS, R. B. 1992. *A Revised Correlation of Silurian Rocks in the British Isles*. Geological Society of London, Special Report **21**, 32 pp.

CORFIELD, R. M., SIVETER, D. J., CARTLIDGE, J. E. & MCKERROW, W. S. 1992. Carbon isotope excursion near the Wenlock-Ludlow, (Silurian) boundary in the Anglo-Welsh area. *Geology* **20**, 371-374.

CRAMER, B. D., CONDON, D. J., SÖDERLUND, U., MARSHALL, C., WORTON, G. W., THOMAS, A. T., CALNER, M., RAY, D. C., PERRIER, V., BOOMER, I., PATCHETT, P. J. & JEPPSSON, L. 2012. U-Pb (zircon) age constraints on the timing and duration of Wenlock (Silurian) paleocommunity collapse and recovery during the 'Big Crisis'. *The Geological Society of America Bulletin* **124** (11/12), 1841-1857.

CRAMER, B. D., BRETT, C. E., MELCHIN, M. A., MÄNNIK, P., KLEFFNER, M. A., MCLAUGHLIN, P. I., LOYDELL, D. K., MUNNECKE, A., JEPPSSON, L., CORRADINI, C., BRUNTON, F. R. & SALTZMAN, M. R. 2011. Revised chronostratigraphic correlation of the Silurian System of North America with global and regional chronostratigraphic units and $\delta^{13}C_{carb}$ chemostratigraphy. *Lethaia* **44**, 185-202.

CRAMER, B. D., KLEFFNER, M. A. & SALTZMAN, M. R. 2006. The Late Wenlock Mulde positive carbon isotope ($\delta^{13}C_{carb}$) excursion in North America. *GFF* **128**, 85-90.

CRAMER, B.D., LOYDELL, D.K., SAMTLEBEN, C., MUNNECKE, A., KALJO, D., MÄNNIK, P., MARTMA, T., JEPPSSON, L., KLEFFNER, M.A., BARRICK, J.E., JOHNSON, C.A., EMSBO, P., JOACHIMSKI, M.M., BICKERT, T., SALTZMAN, M.R., 2010. Testing the limits of Paleozoic chronostratigraphic correlation via high-resolution (<500,000 yrs) integrated conodont, graptolite, and carbon isotope ($\delta^{13}C_{carb}$) biochemostratigraphy across the Llandovery–Wenlock (Silurian) boundary: is a unified Phanerozoic timescale achievable? Geological Society of America Bulletin **122**, 1700–1716.

CRAMER, B. D., VANDENBROUCKE, T. R. A. & LUDVIGSON, G. A. 2015. High-Resolution Event Stratigraphy (HiRES) and the quantification of stratigraphic uncertainty: Silurian examples of the quest for precision in stratigraphy. *Earth-Science Reviews* **141**, 136-153.

DA SILVA, A.-C. & BOULVAIN, F. 2008. Carbon isotope lateral variability in a Middle Frasnian carbonate platform (Belgium): Significance of facies, diagenesis and sea-level history. Palaeogeography, Palaeoclimatology, Palaeoecology 269, 189-204.

DAVIES, J. R., RAY, D. C., THOMAS, A. T., LOYDELL, D. K., CHERNS, L., CRAMER, B. D., VEEVERS, S. J., WORTON, G. J., MARSHALL, C., MOLYNEUX, S. G., VANDENBROUCKE, T.

R. A., Verniers, J., Waters, R. A., Williams, M. & Zalasiewicz, J. A. 2011. Siluria revisited: A field guide. International Subcommission on Silurian Stratigraphy, Field Meeting 2011 (ed. D.C. Ray), 170 pp.

Fry, C. R., Ray, D. C., Wheeley, J. R., Boomer, I., Jarochowska, E. & Loydell, D. K. 2017. The Homerian carbon isotope excursion (Silurian) within graptolitic successions on the Midland Platform (Avalonia), UK: implications for regional and global comparisons and correlations. *GFF* **139** (4), 301-313.

Frýda, J. & Frýdova, B. 2016. The Homerian (late Wenlock, Silurian) carbon isotope excursion from Perunica: Does dolomite control the magnitude of the carbon isotope excursion? *Canadian Journal of Earth Sciences* **53** (7), 695-701.

Holmden, C., Creaser, R. A., Muehlenbachs, K., Leslie, S. A. & Bergstrom, S. M. 1998. Isotopic evidence for geochemical decoupling between ancient epeiric seas and bordering oceans: Implications for secular curves. Geology **26** (6), 567-570

Huff, W. D. 2016. K-bentonites: A review. American Mineralogist **101**, 43-70

Hughes, H. E. & Ray, D. C. 2016. The carbon isotope and sequence stratigraphic record of the Sheinwoodian and lower Homerian stages (Silurian) of the Midland Platform, UK. *Palaeogeography, Palaeoclimatology, Palaeoecology* **445**, 97-114.

Jarochowska, E., Ray, D. C., Röstel, P., Worton, G. & Munnecke, A. 2017. Harnessing stratigraphic bias at the section scale: Conodont diversity in the Homerian

(Silurian) of the Midland Platform, England. *Dryad Digital Repository.* https://doi.org/10.5061/dryad.7sd66

JAROCHOWSKA, E., RAY, D. C., RÖSTEL, P., WORTON, G. & MUNNECKE, A. 2018. Harnessing stratigraphic bias at the section scale: Conodont diversity in the Homerian (Silurian) of the Midland Platform, England. *Palaeontology* **61**, 57-76.

JAROCHOWSKA, E. & MUNNECKE, A. 2015. Silurian carbonate high-energy deposits of potential tsunami origin: Distinguishing lateral redeposition and time averaging using carbon isotope chemostratigraphy. *Sedimentary Geology* **315**, 14-28.

JOHNSON, M. E. 2006. Relationship of Silurian sea fluctuations to oceanic episodes and events. *GFF* **128**, 115-121.

KALJO, D. & MARTMA, T. 2006. Application of carbon isotope stratigraphy to dating the Baltic Silurian rocks. *GFF* **128**, 123-129.

KOZŁOWSKI, W. & SOBIEŃ, K. 2012. Mid-Ludfordian coeval carbon isotope, natural gamma ray and magnetic susceptibility excursions in the Mielnik IG-1 borehole (Eastern Poland)—Dustiness as a possible link between global climate and the Silurian carbon isotope record. *Palaeogeography, Palaeoclimatology, Palaeoecology* **339**, 74-97.

MARSHALL, C., THOMAS, A.T., BOOMER, I. & RAY, D. C. 2012. High resolution $\delta^{13}C$ stratigraphy of the Homerian (Wenlock) of the English Midlands and Wenlock Edge. *Bulletin of Geosciences* **87**, 669-679.

MELCHIN, M. J., SADLER, P. M. & CRAMER, B. D. 2012. The Silurian Period. In *The Geologic Time Scale 2012* (eds F. M. Gradstein, J. G. Ogg, M. Schmitz & G. Ogg), pp. 525-558. Elsevier, New York.

OLIVER, P. G. 1981. Lithological groups within the Wenlock Limestone (Silurian) at Wren's Nest. *The Black Country Geologist, Black Country Geological Society* **1**, 39-53.

PÄßLER, J.-F., JAROCHOWSKA, E., RAY, D. C., MUNNECKE, A. & WORTON, G. J. 2014. Aphanitic buildup from the onset of the Mulde Event (Homerian, middle Silurian) at Whitman's Hill, Herefordshire, UK: ultrastructural insights into proposed microbial fabrics. *Estonian Journal of Earth Sciences* **63**, 287-292.

Peng, S. C. & Babcock, L. E. 2011. Continuing progress on chronostratigraphic subdivision of the Cambrian System. *Bulletin of Geosciences* **86** (3), 391-396.

PENN, J. S. W. 1971. Bioherms in the Wenlock Limestone of the Malvern area (Herefordshire, England). *Mémoires du Bureau de Recherches Géologiques et Minières* **73**, 129-137.

PHIPPS, C. B. & REEVE, F. A. E. 1967. Stratigraphy and geological history of the Malvern, Abberley and Ledbury Hills. *Geological Journal* **5**, 339-368.

PRICE, G. D., FŐZY, I. & PÁLFY J. 2016. Carbon cycle history through the Jurassic–Cretaceous boundary: A new global $\delta^{13}C$ stack. *Palaeogeography, Palaeoclimatology, Palaeoecology* **451**, 46-61.

RAY, D. C., RICHARDS, T. D., BRETT, C. D., MORTON, A. & BROWN, A. M. 2013. Late Wenlock sequence and bentonite stratigraphy in the Malvern, Suckley and Abberley Hills, England. *Palaeogeography, Palaeoclimatology, Palaeoecology* **389**, 115-127.

RAY, D. C. & THOMAS, A. T. 2007. Carbonate depositional environments, sequence stratigraphy and exceptional skeletal preservation in the Much Wenlock Limestone Formation (Silurian) of Dudley, England. *Palaeontology* **50** (1), 197-222.

RAY, D. C., BRETT, C. E., THOMAS, A. T. & COLLINGS, A. V. J. 2010. Late Wenlock sequence stratigraphy in central England. *Geological Magazine* **147** (1), 123-144.

RAY, D. C., COLLINGS, A. V. J., WORTON, G. J. & JONES, G. 2011. Upper Wenlock bentonites from Wren's Nest Hill, Dudley; comparisons with prominent bentonites along Wenlock Edge, Shropshire, England. *Geological Magazine* **148** (4), 670-681.

RATCLIFFE, K. T. 1988. Oncoids as environmental indicators in the Much Wenlock Limestone Formation of the English Midlands. *Journal of the Geological Society, London* **145**, 117-24.

RATCLIFFE, K. T. & THOMAS, A. T. 1999. Carbonate depositional environments in the late Wenlock of England and Wales. *Geological Magazine* **136** (2), 189-204.

SALTZMAN, M. R. & THOMAS, E. 2012. Carbon isotope stratigraphy. In *The Geologic Time Scale 2012* (eds F. M. Gradstein, J. G. Ogg, M. Schmitz & G. Ogg), pp. 207-232. Elsevier, New York.

SIMMONS, M. D. 2012. Sequence Stratigraphy and Sea-Level Change. In: Gradstein, F.M., Ogg, J.G., Schmitz, M., Ogg, G. (Eds.), The Geologic Time Scale 2012. Elsevier, New York, pp. 239–267 (Chapter 13).

STANLEY, G. D. & LIPPS, J. H. 2011. Photosymbiosis: the driving force for reef success and failure. In *Corals and Reef Crises, Collapse and Change* (ed G. D. Stanley), pp. 33-60. Boulder: The Palaeontological Society.

SWART, P. K. 2008. Global synchronous changes in the carbon isotopic composition of carbonate sediments unrelated to changes in the global carbon cycle. PNAS, **105** (37), 13741-13745

TORSVIK, T. H., TRENCH, A., SVENSSON, I. & WALDERHAUG, H. J. 1993. Palaeogeographic significance of mid-Silurian palaeomagnetic results from southern Britain - major revision of the apparent polar wander path for eastern Avalonia. *Geophysical Journal International* **113**, 651-668.

VANDENBERGHE, N., HILGEN, F.J. & SPEIJER R. P. 2012. The Paleogene Period. In *The Geologic Time Scale 2012* (eds F. M. Gradstein, J. G. Ogg, M. Schmitz & G. Ogg), pp. 855-921. Elsevier, New York.

WEISSERT, H, JOACHIMSKI, M. M. & SARNTHEIN, M. 2008. Chemostratigraphy. *Newsletters on Stratigraphy* **42** (3), 145-179.

Supplementary Material

Supplementary Material. $\delta^{13}C_{carb}$ and $\delta^{18}O$ data from Whitman's Hill Quarry, Bruff Business Park, Castle Mill Basin, Reef Knoll Stairwell, Lower NCC Cutting, Seven Sisters Quarry North, Upper NCC Cutting, Reef Knoll Quarry, Snake Pit Quarry and Lion's Mouth Cavern.

Supplementary Material: δ13Ccarb and δ18O data from Whitman's Hill Quarry, Bruff Business Park, Castle Mill Basin, Reef Knoll Stairwell, Lower NCC Cutting, Seven Sisters Quarry North, Upper NCC Cutting, Reef Knoll Quarry, Snake Pit Quarry and Lion's Mouth Cavern.

Whitmans Hill (WHI)

Sample Code	Position from lowest sample (m)	$\delta^{13}C$	$\delta^{18}O$
WHI001	0.00	-0.9	-7.0
WHI002	0.13	0.0	-7.4
WHI003	0.72	-1.2	-6.9
WHI004	1.00	-1.3	-6.8
WHI005	1.53	-0.2	-8.4
WHI006	2.87	-0.1	-7.8
WHI007	3.94	-1.3	-7.1
WHI008	5.93	0.6	-7.2
WHI009	7.20	0.3	-6.9
WHI010	8.29	-0.4	-7.4
WHI011	9.89	0.9	-7.4
WHI012	11.30	0.2	-7.3
WHI013	11.50	0.2	-7.1
WHI014	11.70	0.4	-7.5
WHI015	11.90	0.3	-7.4
WHI016	12.10	0.3	-7.5
WHI017	12.30	0.3	-7.8
WHI018	13.44	0.6	-7.0
WHI019	13.64	0.8	-6.7
WHI020	13.84	0.7	-7.0
WHI021	14.04	0.7	-7.0
WHI022	14.24	-0.2	-4.6
WHI023	14.44	0.9	-5.9
WHI024	14.64	1.2	-6.3
WHI025	14.84	0.8	-6.7
WHI026	15.04	1.0	-6.4
WHI027	15.24	0.9	-6.0
WHI028	15.44	1.8	-6.1
WHI029	15.64	0.9	-6.5
WHI030	15.74	2.0	-4.8
WHI031	15.84	1.3	-6.7
WHI032	15.89	1.5	-6.7
WHI033	15.94	2.7	-5.8
WHI034	15.99	2.7	-6.1
WHI035	16.04	1.3	-7.8
WHI036	16.09	2.1	-6.5
WHI037	16.14	3.6	-6.6
WHI038	16.24	3.9	-7.4
WHI039	16.34	4.6	-6.3
WHI040	16.44	4.5	-7.4
WHI041	16.54	4.6	-6.9
WHI042	16.64	4.2	-8.6
WHI043	16.74	4.0	-6.5
WHI044	16.84	4.2	-7.5
WHI045	17.00	3.6	-6.9
WHI046	17.04	4.3	-6.2
WHI047	17.13	4.6	-5.2
WHI048	17.22	4.8	-5.2
WHI049	17.31	4.4	-7.7
WHI050	17.40	4.5	-7.2
WHI051	17.49	4.4	-7.3
WHI052	17.58	4.8	-5.9
WHI053	17.67	4.0	-7.7
WHI054	17.76	4.0	-4.5
WHI055	17.85	4.6	-5.6
WHI056	17.94	4.3	-6.1
WHI057	18.14	4.2	-6.9
WHI058	18.24	4.5	-6.3
WHI059	18.34	4.1	-5.3
WHI060	18.44	4.6	-6.4
WHI061	18.54	3.5	-9.8
WHI062	18.64	3.4	-6.5
WHI063	18.74	3.7	-6.6
WHI064	18.84	4.1	-5.6
WHI065	18.94	4.3	-6.7
WHI066	19.04	4.2	-7.7
WHI067	19.14	4.2	-7.8
WHI068	19.24	4.4	-7.0
WHI069	19.34	3.9	-6.1
WHI070	19.44	4.1	-5.9
WHI071	19.55	4.1	-7.7
WHI072	19.66	3.8	-6.0
WHI073	19.77	4.1	-6.5
WHI074	19.88	2.9	-6.9
WHI075	19.99	3.9	-5.9
WHI076	20.10	3.7	-5.5
WHI077	20.21	4.2	-6.0
WHI078	20.32	4.2	-6.7
WHI079	20.52	4.0	-6.1
WHI080	20.72	2.9	-5.9
WHI081	20.92	3.9	-5.4
WHI082	21.12	3.9	-5.9
WHI083	21.32	3.5	-6.1
WHI084	21.52	4.0	-5.7
WHI085	21.72	3.9	-5.7
WHI086	21.92	3.8	-5.5
WHI087	22.12	3.9	-6.9
WHI088	22.32	2.9	-6.2
WHI089	22.52	3.3	-5.2
WHI090	22.72	4.0	-5.3
WHI091	22.92	3.8	-5.2
WHI092	23.12	4.0	-5.6
WHI093	23.32	3.9	-5.7
WHI094	23.52	3.6	-5.3
WHI095	23.72	3.5	-5.5
WHI096	23.92	3.8	-6.8
WHI097	24.12	3.8	-6.4
WHI098	24.32	3.8	-6.2
WHI099	24.49	3.7	-6.1
WHI100	24.69	3.6	-6.6
WHI101	24.89	3.4	-6.9
WHI102	25.09	3.6	-6.3
WHI103	25.29	3.6	-6.5
WHI104	25.49	3.6	-6.2
WHI105	25.69	2.9	-8.0
WHI106	25.89	3.2	-7.2
WHI107	26.09	3.2	-6.8
WHI108	26.54	1.8	-7.8
WHI109	26.79	3.3	-6.7
WHI110	26.99	3.2	-6.7
WHI111	27.19	3.3	-7.1
WHI112	27.39	3.2	-6.2
WHI113	27.59	3.2	-6.3
WHI114	27.79	3.2	-6.3
WHI115	28.13	3.0	-7.4
WHI116	28.32	3.2	-6.5
WHI117	28.52	3.2	-6.3
WHI118	28.67	3.0	-6.1
WHI119	28.72	3.0	-6.1
WHI120	28.92	3.1	-6.2
WHI121	29.12	2.9	-6.0
WHI122	29.32	2.5	-6.1
WHI123	29.52	3.0	-6.0
WHI124	29.72	3.0	-5.8
WHI125	29.92	3.0	-5.9
WHI126	30.12	3.1	-6.1
WHI127	30.32	2.8	-5.9
WHI128	30.52	2.9	-6.8
WHI129	30.72	2.7	-6.2
WHI130	30.92	2.7	-7.0
WHI131	31.12	2.8	-6.2
WHI132	31.32	2.6	-6.9
WHI133	31.52	1.5	-7.8
WHI134	31.72	2.8	-6.5
WHI135	31.92	1.9	-6.7
WHI136	32.12	2.5	-6.3
WHI137	32.32	2.1	-6.4
WHI138	32.52	2.3	-6.2
WHI139	32.72	2.4	-6.4
WHI140	32.92	2.0	-6.0
WHI141	33.12	2.7	-6.8
WHI142	33.32	2.7	-6.5
WHI143	33.52	2.7	-6.4
WHI144	33.72	2.8	-6.3
WHI145	33.92	2.7	-6.5
WHI146	34.17	2.6	-6.3
WHI147	34.34	2.6	-7.6
WHI148	34.82	2.6	-6.7
WHI149	35.02	2.3	-6.3
WHI150	35.22	2.2	-6.9
WHI151	35.42	2.4	-7.0
WHI152	35.62	2.3	-6.4
WHI153	35.82	2.0	-6.8
WHI154	36.02	2.4	-6.6
WHI155	36.22	2.4	-6.3
WHI156	36.42	2.4	-6.6
WHI157	36.62	2.1	-7.5
WHI158	36.82	2.0	-7.1
WHI159	37.02	2.0	-5.9
WHI160	37.22	1.9	-6.0
WHI161	37.42	2.0	-6.1
WHI162	37.62	2.1	-6.2
WHI163	37.82	1.6	-6.7
WHI164	38.02	1.9	-7.0
WHI165	38.22	2.0	-5.6
WHI166	38.42	2.0	-5.2
WHI167	38.62	2.0	-6.6
WHI168	38.82	1.3	-6.5
WHI169	39.02	0.9	-8.9
WHI170	39.22	1.9	-6.9
WHI171	39.42	1.9	-6.1
WHI172	39.62	1.2	-6.3
WHI173	39.82	1.9	-6.6
WHI174	40.02	1.9	-5.8
WHI175	40.22	2.1	-5.4

Bruff Business Park (BBP)

Sample Code	Position from lowest sample (m)	$\delta^{13}C$	$\delta^{18}O$
BBP001	0.00	2.1	-7.4
BBP002	0.55	2.4	-6.7
BBP003	1.05	2.5	-6.5
BBP004	1.55	2.4	-6.0
BBP005	2.05	2.5	-6.5
BBP006	2.55	2.8	-6.4
BBP007	3.05	2.3	-6.6
BBP008	3.55	2.4	-5.9
BBP009	4.05	2.4	-6.8
BBP010	4.55	2.4	-5.7
BBP011	5.05	2.2	-6.6
BBP012	5.55	2.2	-6.1
BBP013	5.80	1.9	-6.0
BBP014	6.05	1.6	-5.7
BBP015	6.25	1.8	-6.2
BBP016	6.50	2.2	-5.9
BBP017	6.75	2.0	-5.9
BBP018	7.00	2.2	-6.0
BBP019	7.20	2.0	-7.8
BBP020	7.40	2.0	-6.9
BBP021	7.60	2.0	-6.7
BBP022	7.85	2.0	-6.5
BBP023	8.10	1.9	-6.5
BBP024	8.25	2.0	-6.8
BBP025	8.60	1.3	-6.6
BBP026	8.85	1.9	-6.0
BBP027	9.10	1.8	-6.6
BBP028	9.35	1.8	-6.6
BBP029	9.60	1.7	-5.7
BBP030	9.85	2.2	-5.7
BBP031	10.10	2.0	-6.4
BBP032	10.35	2.1	-5.7
BBP033	10.60	2.0	-6.5
BBP034	10.85	2.3	-5.4
BBP035	11.10	2.0	-5.6
BBP036	11.35	2.2	-5.5
BBP037	11.60	2.4	-5.8
BBP038	11.85	2.0	-5.8
BBP039	12.10	2.6	-5.9
BBP040	12.35	2.7	-5.1
BBP041	12.60	2.7	-6.2
BBP042	12.85	2.7	-6.1
BBP043	13.10	2.5	-6.5
BBP044	13.35	2.8	-5.6
BBP045	13.60	2.6	-6.3
BBP046	13.85	2.3	-8.0
BBP047	14.10	2.8	-7.8
BBP048	14.35	2.6	-7.8
BBP049	14.60	2.8	-5.9
BBP050	14.85	2.5	-7.2
BBP051	15.10	3.0	-6.1
BBP052	15.35	2.6	-5.8
BBP053	15.60	2.2	-5.5
BBP054	15.85	2.7	-6.4
BBP055	16.10	2.9	-6.3
BBP056	16.35	2.6	-6.3
BBP057	16.60	2.7	-6.0
BBP058	16.85	2.4	-6.1
BBP059	17.10	2.8	-6.1
BBP060	17.35	2.5	-6.1
BBP061	17.60	2.7	-6.4
BBP062	17.85	2.3	-6.2
BBP063	18.35	2.3	-6.6
BBP064	18.80	2.4	-6.3
BBP065	19.15	2.4	-6.1
BBP066	19.45	2.3	-6.6
BBP067	19.70	2.3	-5.9
BBP068	20.00	2.2	-6.6
BBP069	20.30	2.4	-6.3
BBP070	20.55	2.2	-6.0
BBP071	20.80	2.0	-6.4
BBP072	21.05	2.2	-5.9
BBP073	21.30	1.7	-6.2
BBP074	21.55	1.8	-6.3
BBP075	21.87	2.0	-6.3
BBP076	22.15	1.3	-6.7
BBP077	22.40	1.8	-6.5
BBP078	22.65	1.1	-6.5
BBP079	22.90	1.9	-7.1
BBP080	23.15	1.9	-6.1
BBP081	23.40	1.8	-6.8
BBP082	23.65	1.5	-7.6
BBP083	23.90	1.4	-6.1
BBP084	24.10	1.2	-5.9
BBP085	24.40	1.4	-7.3
BBP086	24.65	1.8	-6.4
BBP087	24.90	1.8	-6.0
BBP088	25.30	1.7	-6.5
BBP089	25.55	1.0	-7.7
BBP090	25.80	1.3	-6.6
BBP091	26.05	1.5	-6.4
BBP092	26.30	1.6	-5.4
BBP093	26.55	1.5	-6.1
BBP094	26.80	1.5	-6.1
BBP095	27.05	1.4	-6.1
BBP096	27.55	1.7	-6.4
BBP097	28.05	1.2	-7.6
BBP098	28.55	1.3	-6.2
BBP099	29.05	1.5	-6.9
BBP100	29.55	1.7	-6.6
BBP101	30.05	1.6	-6.1

Castle Mill Basin (CMB)

Sample Code	Position from lowest sample (m)	$\delta^{13}C$	$\delta^{18}O$
CMB001	0.00	0.9	-6.3
CMB002	0.20	0.8	-6.1
CMB003	0.40	1.0	-5.5
CMB004	0.60	1.2	-5.2
CMB005	0.70	1.2	-6.0
CMB006	0.80	1.5	-5.1
CMB007	0.90	1.4	-4.8
CMB008	1.00	1.4	-6.5
CMB009	1.10	1.5	-6.1
CMB010	1.20	1.4	-5.7
CMB011	1.30	1.7	-5.5
CMB012	1.40	1.4	-5.2
CMB013	1.50	2.0	-5.6
CMB014	1.60	2.1	-4.6
CMB015	1.75	2.3	-4.6
CMB016	1.90	2.4	-4.8
CMB017	2.00	2.4	-5.6
CMB018	2.10	2.4	-5.0
CMB019	2.20	2.5	-4.7
CMB020	2.30	2.6	-5.2
CMB021	2.40	2.7	-5.1
CMB022	2.50	2.6	-6.7
CMB023	2.60	3.1	-5.4
CMB024	3.60	3.6	-9.5
CMB025	3.80	3.9	-6.0
CMB026	4.00	3.5	-6.3
CMB027	4.20	3.9	-7.1
CMB028	4.40	3.5	-8.4
CMB029	4.60	1.2	-7.4
CMB030	4.80	2.3	-9.4
CMB031	5.00	-0.8	-8.1
CMB032	5.20	3.8	-5.8
CMB033	5.40	2.0	-7.4
CMB034	5.60	4.2	-6.1
CMB035	5.80	2.5	-9.2
CMB036	6.20	3.7	-6.8
CMB037	6.40	3.6	-10.2
CMB038	6.60	3.0	-7.7
CMB039	6.80	1.7	-8.5
CMB040	7.00	4.0	-6.1
CMB041	7.20	2.3	-8.6
CMB042	7.40	4.1	-7.6
CMB043	7.60	4.4	-6.0
CMB044	7.80	4.2	-6.2
CMB045	8.10	4.2	-4.5
CMB046	8.20	3.2	-5.8
CMB047	8.80	4.0	-6.6

Reef Knoll Steps Section (RKS)

Sample Code	Position from lowest sample (m)	$\delta^{13}C$	$\delta^{18}O$
RKS001	0.00	0.7	-7.8
RKS002	0.04	0.7	-7.1
RKS003	0.08	-0.2	-7.5
RKS004	0.1	0.5	-6.3
RKS005	0.13	0.8	-6.2
RKS006	0.19	0.9	-5.4
RKS007	0.24	0.9	-6.2
RKS008	0.28	1.0	-7.4
RKS009	0.31	1.1	-5.7
RKS010	0.36	0.7	-5.9
RKS011	0.42	1.7	-5.4
RKS012	0.45	1.4	-7.0
RKS013	0.49	1.6	-5.5
RKS014	0.56	1.9	-5.1
RKS015	0.58	1.8	-5.6
RKS016	0.62	1.6	-6.2
RKS017	0.68	2.1	-4.8

Lower NCC Cutting (LNC)

Sample Code	Position from lowest sample (m)	$\delta^{13}C$	$\delta^{18}O$
LNC001	0.00	4.8	-6.7
LNC002	0.50	5.2	-5.3
LNC003	1.00	5.0	-6.5
LNC004	1.50	5.5	-5.6
LNC005	2.00	5.5	-6.1
LNC006	3.00	5.5	-6.7
LNC007	3.50	3.9	-8.4
LNC008	4.00	4.9	-6.8
LNC009	4.50	5.4	-6.7
LNC010	5.00	5.1	-6.7
LNC011	5.50	2.9	-8.4
LNC012	5.75	5.0	-7.0
LNC013	6.25	4.9	-6.2
LNC014	6.75	2.5	-6.1
LNC015	7.00	4.2	-6.0
LNC016	7.25	3.5	-7.2
LNC017	7.50	3.5	-7.2
LNC018	7.75	3.0	-7.8

Seven Sisters Quarry North (SSQ)

Sample Code	Position from lowest sample (m)	$\delta^{13}C$	$\delta^{18}O$
SSQ001	0.00	3.3	-6.1
SSQ002	0.50	3.1	-6.8
SSQ003	1.00	3.5	-5.5
SSQ004	1.50	3.1	-6.8
SSQ005	2.00	3.1	-6.2
SSQ006	2.50	2.8	-7.3
SSQ007	3.00	2.5	-7.1
SSQ008	3.50	2.2	-6.7
SSQ009	4.00	2.2	-6.5

Upper NCC Cutting (UNC)

Sample Code	Position from lowest sample (m)	$\delta^{13}C$	$\delta^{18}O$
UNC001	0.00	1.1	-9.5
UNC002	0.50	1.2	-5.6
UNC003	1.00	1.7	-7.7
UNC004	1.50	1.2	-6.4
UNC005	2.00	0.5	-8.7
UNC006	2.50	0.9	-6.7
UNC007	3.00	1.0	-7.1
UNC008	3.50	0.7	-7.6
UNC009	4.00	-0.6	-7.7
UNC010	4.50	-0.4	-9.5
UNC011	5.00	0.2	-8.2
UNC012	5.50	2.0	-5.9
UNC013	5.75	2.0	-6.9
UNC014	6.25	2.5	-6.7
UNC015	6.75	2.5	-6.9
UNC016	7.25	2.4	-6.9
UNC017	7.50	2.6	-5.7
UNC018	7.75	2.5	-5.4
UNC019	8.00	2.3	-5.7
UNC020	8.50	2.4	-6.0
UNC021	9.00	1.7	-8.0
UNC022	9.50	2.2	-6.8
UNC023	10.00	2.0	-6.0
UNC024	10.50	1.8	-5.1
UNC025	11.00	2.2	-5.3
UNC026	11.50	2.4	-5.4
UNC027	12.00	2.7	-4.6
UNC028	12.50	2.5	-6.4
UNC029	13.00	2.8	-5.8
UNC030	13.50	3.1	-5.6
UNC031	14.00	2.9	-5.8
UNC032	14.50	3.0	-6.1

Reef Knoll Quarry RKQ

Sample Code	Position from lowest sample (m)	$\delta^{13}C$	$\delta^{18}O$
RKQ001	0.00	2.8	-6.3
RKQ002	0.50	2.9	-5.9
RKQ003	1.00	3.0	-6.5
RKQ004	1.50	3.6	-6.4
RKQ005	2.00	3.5	-5.6
RKQ006	2.50	3.7	-6.0
RKQ007	3.00	3.8	-5.9
RKQ008	3.50	3.8	-5.6
RKQ009	4.00	3.8	-5.3
RKQ010	4.50	3.6	-5.8
RKQ011	5.00	3.3	-7.3
RKQ012	5.50	3.5	-6.2
RKQ013	6.00	3.4	-6.0
RKQ014	6.50	3.3	-6.1
RKQ015	7.00	3.4	-6.3
RKQ016	7.50	3.2	-6.1
RKQ017	8.00	3.2	-6.1
RKQ018	8.50	3.1	-5.7
RKQ019	9.00	2.8	-6.8
RKQ020	9.50	2.9	-6.7
RKQ021	10.00	2.7	-6.0
RKQ022	10.50	1.9	-6.2
RKQ023	11.00	2.0	-6.3

Snake Pit Quarry (SPQ)

Sample Code	Position from lowest sample (m)	$\delta^{13}C$	$\delta^{18}O$
SPQ001	0.00	2.2	-6.3
SPQ002	0.50	1.1	-9.5
SPQ003	1.00	2.3	-6.1
SPQ004	1.50	2.4	-6.7
SPQ005	2.00	1.1	-7.8
SPQ006	2.50	2.3	-7.6
SPQ007	3.00	2.3	-7.7
SPQ008	3.50	2.2	-8.2
SPQ009	4.00	2.1	-6.6
SPQ010	4.50	2.1	-6.8
SPQ011	5.00	2.1	-8.4
SPQ012	5.50	2.0	-8.2
SPQ013	6.00	1.8	-9.0
SPQ014	6.50	1.0	-7.7

Lion's Mouth Cavern (LMC)

Sample Code	Position from lowest sample (m)	$\delta^{13}C$	$\delta^{18}O$
LMC001	0.00	2.2	-8.3
LMC002	0.21	2.0	-7.4
LMC003	0.44	2.1	-7.2
LMC004	0.68	2.0	-8.6
LMC005	0.95	2.1	-8.7
LMC006	1.12	2.2	-7.6
LMC007	1.41	2.1	-7.6
LMC008	1.68	1.9	-7.7
LMC009	1.95	1.1	-9.2
LMC010	2.09	1.3	-8.9
LMC011	2.26	0.9	-6.6
LMC012	2.44	0.9	-6.5
LMC013	2.71	0.6	-8.3
LMC014	2.90	1.0	-7.6
LMC015	3.07	1.2	-9.2
LMC016	3.30	0.9	-7.5
LMC017	3.50	0.7	-8.4
LMC018	3.66	0.5	-6.3
LMC019	3.80	0.4	-7.2
LMC020	4.00	0.5	-6.4
LMC021	4.21	0.2	-6.8
LMC022	4.43	0.3	-6.5
LMC023	4.63	0.2	-6.2